Journal of Dynamics, Monitoring and Diagnostics, 2026, 5, 1-24
https://doi.org/10.37965/jdmd.2026.1133

ISTP
RESEARCH ARTICLE

Performance Evaluation of Smart Home Digital Twins: A Thermal Comfort Case Study

Aminu E. Isiyaku, Mubarak Aderibigbe, Rakesh Mishra, and Anshu Gaur
School of Computing and Engineering, University of Huddersfield, Huddersfield, UK

(Received 08 January 2026; Revised 10 March 2026; Accepted 11 March 2026; Published online 13 March 2026)

Abstract: Decarbonising residential buildings requires control strategies that can maintain thermal comfort while minimising energy use. Traditional rule-based HVAC controls often fall short, as they struggle to respond to rapidly changing indoor conditions and evolving energy constraints. This study presents a real-time digital twin (DT) framework for optimising thermal comfort in smart homes, combining low-cost IoT sensing, computational fluid dynamics (CFD) simulation (ANSYS Fluent), and dynamic control algorithms implemented in MATLAB. The framework was validated in an occupied residential setting using a structured key performance indicator (KPI) approach across eight scenarios with varying window apertures (0–0.3 m) under passive and active heating and ventilation modes. Performance was assessed using ISO 7730 comfort metrics (Predicted Mean Vote (PMV) and Predicted Percentage Dissatisfied (PPD)), statistical accuracy indicators (mean absolute error, root mean square error, and R^2), and operational feasibility measures (latency, spatial consistency, cost efficiency). The system achieved PMV targets in 88% of cases, with full compliance (<10% PPD). Passive ventilation scenarios showed the strongest comfort performance and favorable practical deployment characteristics, while energy-related outcomes remained scenario-dependent. Predictive reliability was supported by Wilcoxon signed-rank tests ($p > 0.05$ in 53% of cases). Overall, the proposed KPI-driven DT framework offers an occupant-responsive and scalable solution for real-time residential thermal comfort management, while also clarifying the conditions required for broader energy benefits to be realised.

Keywords: computational fluid dynamics; digital twin; heating dynamics; IoT sensors; KPI framework, real-time control; thermal comfort; smart home validation

I. INTRODUCTION

A. GENERAL BACKGROUND

Buildings currently account for approximately 40% of global energy consumption and contribute around 36% of global CO_2 emissions. This positions them prominently in international sustainability strategies, notably aligning with the United Nations Sustainable Development Goals (SDGs) such as SDG 7 (Affordable and Clean Energy) and SDG 11 (Sustainable Cities and Communities), while also aligning with global sustainability targets outlined in the International Energy Agency's Net Zero by 2050 roadmap [1].

Conventional HVAC systems predominantly operate on fixed control schemes and reactive feedback mechanisms, significantly limiting their flexibility and adaptability, thus constraining their ability to simultaneously optimise energy performance and occupant thermal comfort [1]. The challenge of achieving optimal energy efficiency and thermal comfort is further exacerbated by fluctuating energy prices, increasingly unpredictable climatic conditions, and growing mandates for building decarbonisation [2].

Emerging as a compelling solution, digital twin (DT) systems serve as dynamic digital replicas of physical buildings, continuously synchronising virtual models with real-world conditions. This advanced capability facilitates predictive thermal modelling, adaptive management of ventilation, and intelligent optimisation of energy flows [2,4]. Despite their considerable potential, the successful implementation of DT-based solutions critically hinges on robust and comprehensive performance metrics [4]. This distinction is important because, unlike machinery-focused DT studies where diagnostic reliability is the main objective, residential comfort DTs must also demonstrate room-scale spatial validity, operational responsiveness, and compliance with recognised thermal comfort standards [5,6].

These approaches typically neglect a holistic consideration of essential operational dimensions, such as spatial accuracy, responsiveness under varying operational conditions, and detailed cost–benefit analyses, leading to incomplete assessments of real-world effectiveness[3,7].

This issue is further compounded by the absence of standardised, domain-specific key performance indicators (KPIs) explicitly designed for residential DT systems. Although existing frameworks, such as ISO 7730, provide validated metrics for thermal comfort evaluation, these frameworks lack integration with critical operational dimensions. These operational dimensions encompass real-time responsiveness and accuracy across different spatial scales and varying environmental conditions, all crucial to effective IoT-enabled residential environments [5,6]. Specifically, system latency, local-to-global predictive accuracy, and cost efficiency (CE) remain significantly underrepresented, resulting in fragmented performance evaluations that inadequately reflect real-world residential conditions.

To address these gaps, this study introduces a structured KPI framework tailored explicitly for evaluating, optimising, and benchmarking residential DT systems, particularly focusing on thermal comfort management.

Corresponding author: Aminu E. Isiyaku (e-mail: aminu.isiyaku@hud.ac.uk).

Anchored in the widely recognised ISO 7730 standard and validated through real-world implementation, this comprehensive framework incorporates quantitative indicators across four critical interdependent domains: thermal comfort, energy efficiency, system responsiveness, and economic viability.

The primary objective of this research is to establish a scalable, transparent evaluation methodology that enables researchers and stakeholders within residential contexts to balance occupant satisfaction, energy optimisation, and cost–effectiveness. By integrating live sensor data, computational fluid dynamics (CFD)-driven simulation, and systematic KPI-based assessment, the framework has potential to provide enhanced predictive reliability and operational adaptability, supporting diverse residential configurations and varied climatic scenarios.

Moreover, clearly defined and robust KPIs provide essential benefits for the continued development and refinement of DT technology. Specifically, standardised KPIs enable consistent benchmarking, systematic performance improvements, and ensure effective translation of DT solutions from research environments into practical residential applications, thereby facilitating broad adoption and maximizing their utility in advancing sustainable building management.

B. THEORETICAL FOUNDATIONS AND TECHNOLOGY ENABLERS OF DIGITAL TWINS

Initially developed for aerospace and industrial applications, DTs have significantly evolved, demonstrating applicability across diverse sectors through continuous processing and integration of real-time sensor data to reflect evolving physical states [7–10].

Contemporary DT architecture predominantly rests upon three critical technological foundations:

1. High-accuracy computational modelling, which accurately represents physical phenomena, material properties, and complex interactions within physical systems.
2. Continuous IoT-enabled data acquisition, ensuring timely and precise monitoring and synchronisation of real-world conditions.
3. Adaptive learning algorithms, leveraging machine learning techniques to provide predictive analytics and prescriptive, real-time decision-making capabilities [9,11].

Practical implementations clearly demonstrate these capabilities. In smart manufacturing, for instance, edge-computing-driven DTs process machining data in real time, enabling instantaneous adjustments to machining parameters within milliseconds [12]. Similarly, in civil infrastructure management, integrating LiDAR scanning with Building Information Modelling (BIM) allows for the accurate simulation and analysis of structural responses to dynamic loads and thermal variations [13].

The scalability and interoperability of DT systems depend significantly on standardised communication protocols and semantic frameworks. Notably, standards like ISO 23247 (“Digital Twin Framework for Manufacturing”) and ontology-based semantic approaches facilitate seamless data integration and interoperability across diverse devices, including CNC machines, robotic systems, and HVAC infrastructure [14]. However, detailed computational models inherent in DT systems substantially increase computational demand, representing a critical scalability challenge.

Recent advancements in federated learning effectively address these computational bottlenecks. Federated learning distributes data analytics across local DT nodes, sharing only aggregated model updates, thereby maintaining data security, reducing centralised computational demands, and significantly enhancing system scalability [15]. Collectively, these developments transform DTs from passive monitoring tools into predictive decision-support platforms, capable of simulating future operational states and guiding informed real-time decision-making within complex building systems.

C. KPI INTEGRATION: BRIDGING DATA AND DECISION-MAKING

Within DT-driven applications, KPIs function as essential abstraction layers, translating raw sensor data into actionable, interpretable metrics that inform real-time decision-making processes. In manufacturing contexts, for example, unit-level energy consumption and dimensional tolerances serve as key indicators guiding system optimisation and continuous improvement efforts [16].

Infrastructure projects further illustrate effective KPI utilization within DT frameworks. A notable example is the Horizon 2020 ASHVIN project, which employs a comprehensive set of KPIs to monitor infrastructure performance across domains such as productivity, resource efficiency, and predictive maintenance. Specifically, the ASHVIN framework employs KPIs such as the Pavement Condition Index, which aggregates sensor data to prioritize infrastructure maintenance interventions and facilitate predictive maintenance strategies [2]. It is important to clearly distinguish between general KPIs used directly for DT evaluation (such as prediction accuracy and latency) and domain-specific KPIs (such as the Pavement Condition Index) used for targeted infrastructure assessment.

For instance, UAV-based inspections in transportation infrastructure projects generate detailed defect maps, feeding into dynamic interfaces that assign risk scores to inform repair scheduling. This hierarchical processing of raw sensor data into intermediate performance indicators and, subsequently, strategic KPIs emphasises the necessity of having a universally recognised and standardised KPI taxonomy. Specifically, in residential DT applications, KPIs must extend beyond purely technical performance metrics to incorporate critical factors such as economic viability and occupant comfort [17].

D. ISO 7730 COMPLIANCE AND KPI-BASED VALIDATION

ISO 7730:2005 provides a validated quantitative framework for assessing thermal comfort, employing two widely recognised indices: the Predicted Mean Vote (PMV) and the Predicted Percentage Dissatisfied (PPD). These indices comprehensively integrate environmental and physiological variables including air temperature, humidity, radiant heat, air velocity, metabolic rates, and clothing insulation to establish defined thresholds for thermal acceptability, often

applied in thermal control compliance checks and system calibration [18].

Recent advancements in DT applications have repositioned PMV and PPD as core KPIs for continuous, real-time thermal comfort evaluation and DT model validation [19]. For instance, structured KPI frameworks integrating PMV and PPD are used to maintain alignment between simulated conditions and real-world environments, even under dynamically changing operational states [19]. Within multi-objective optimisation strategies, PMV and PPD metrics, alongside other KPIs such as energy savings and response latency, serve as integral elements guiding real-time decision-making and ensuring occupant comfort compliance [20].

Further, thresholds derived directly from ISO 7730 standards such as maintaining a PPD $\leq 10\%$ have been operationalized as critical regulatory constraints within advanced DT control frameworks. This practice elevates ISO 7730 from merely a compliance benchmark to an embedded, algorithm-driven performance reference that continuously guides and validates DT systems for comfort-focused building operations [19].

E. BENCHMARKING DIGITAL TWINS: CORE PERFORMANCE METRICS

A particular systematic approach was introduced by Psarommatis and May [4], who propose a comprehensive framework comprising clearly defined, quantifiable metrics designed to evaluate both predictive accuracy and computational responsiveness of DT implementations. The categorization of metrics was structured into distinct performance groups namely Accuracy, Repeatability, and Computational Response which facilitate ease of replication and practical deployment.

Figure 1 illustrates generic KPIs accompanied by their mathematical formulations used for assessing DT operational performance, adapted from the methodology proposed by Psarommatis and May [4]. Three critical dimensions are presented: accuracy, repeatability, and computational response. The Accuracy of Each Output Parameter (AOP_y) quantifies the relative error between predicted and actual DT outputs, where $X_{y,R,i}$ and $X_{y,DT,i}$ are the real and DT-predicted values, respectively, with N being the number of experimental measurements. The Global DT Accuracy ($GDTA$) aggregates individual accuracy metrics across all output parameters. For Repeatability, the Accuracy Variance ($ACVAR_y$) assesses the consistency of DT predictions across multiple runs for a single parameter, with its global equivalent ($GAVAR$) calculated by averaging $ACVAR$ values. Lastly, the Computational Response of the DT is evaluated by measuring both the Average Response Time (ART) and the Response Time Variance ($RTVAR$), reflecting computational efficiency and stability under varying input conditions. Collectively, these KPIs provide a quantitative framework for systematically evaluating and validating DT implementations.

F. FRAMEWORK: IMPLEMENTATION AND VALIDATION APPROACH

The proposed DT performance evaluation framework was implemented and validated within a live smart home

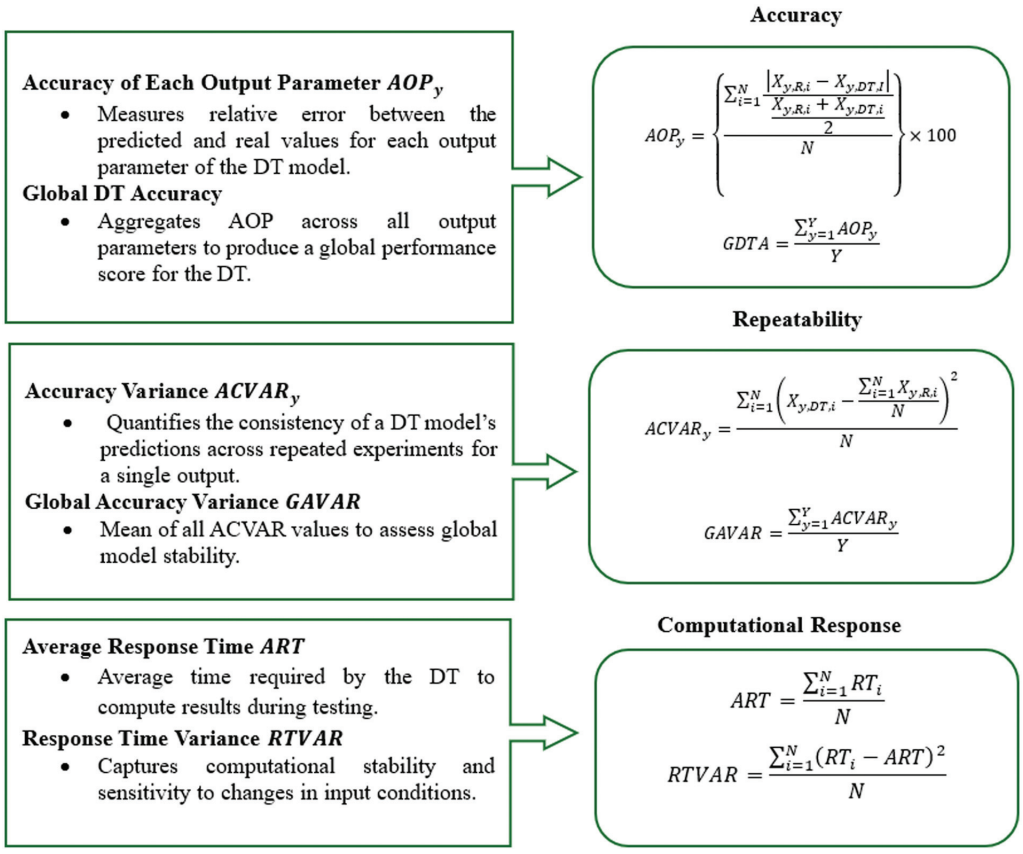

Fig. 1. Generic key performance indicators (KPIs) and mathematical formulations for evaluating digital twin operational performance [4].

environment, integrating a multi-dimensional KPI structure that spans both domain-specific and generic assessment categories. The framework systematically evaluated the DT's effectiveness across four core domains: thermal comfort, energy efficiency, system reliability, and operational feasibility, thereby enabling a holistic characterization of its predictive precision, responsiveness, and deployment readiness.

Thermal comfort was assessed using ISO 7730 aligned metrics PMV and PPD with validation targets set at PMV within ± 0.5 and PPD below 10%, ensuring compliance with international thermal comfort standards.

Energy-related performance was assessed as contextual information to show how the comfort-led control strategy behaved under different operating conditions. These outcomes were benchmarked against the sensor-only baseline controller, but they are interpreted cautiously because short-duration tests, seasonal effects, and ventilation-heating trade-offs can strongly influence the net result.

System reliability was evaluated using statistical metrics comparing simulation outputs to real sensor data under diverse environmental conditions. Validation employed mean absolute error (MAE), root mean square error (RMSE), coefficient of determination, and the Wilcoxon signed-rank test, each reflecting predictive accuracy and internal consistency.

Operational feasibility, critical for deployment scalability, was assessed using four key indicators:

- System Latency (s): Full closed-loop latency (simulation-to-actuation) and edge-level responsiveness, enabling real-time actuation in dynamic control contexts.
- Local-to-Global Accuracy Ratio: Captured spatial consistency between on-site sensor readings and spatially interpolated CFD predictions.
- Operational Range: Assessed stability and performance robustness under variable occupancy profiles and environmental conditions.
- Cost Efficiency: Evaluated the economic viability of the DT system by relating deployment costs to energy savings and control performance.

This integrated, KPI-centric framework facilitated comprehensive DT validation within a realistic residential environment. Its modular structure allows for transparent benchmarking and cross-study reproducibility, while also demonstrating scalability and decision-support capabilities suitable for advanced thermal and energy management in smart buildings.

Table I outlines a structured KPI framework for evaluating DT performance in smart residential thermal and energy management. The framework categorizes indicators into four key domains: thermal comfort, energy efficiency, system reliability, and operational feasibility, thereby supporting a comprehensive assessment of both predictive accuracy and deployment viability. This cross-domain integration confirms the DT's capability to deliver

Table I. Key performance indicators (KPIs) applied in the smart digital twin framework for thermal comfort evaluation and practical deployment assessment

KPI category	Performance indicator (PI)	Description	Recent supporting literature
Thermal comfort (*non-generic*)	Predicted Mean Vote (PMV)	Captures thermal sensation as per ISO 7730; MAE ≤ 0.15 ensures comfort band alignment.	[19,21–23]
	Predicted Percentage Dissatisfied (PPD)	Indicates percentage of occupants dissatisfied; threshold PPD < 10% used to maintain comfort.	[19,21,24]
Energy efficiency *(non-generic)*	Energy savings (%)	Measures HVAC energy reduction due to adaptive DT control.	
System reliability (*generic*)	Mean absolute error (MAE)	Measures average deviation between simulated and actual temperatures.	[21,22,25,26]
	Root mean square error (RMSE)	Penalizes large errors more strongly; RMSE ≤ 2.0 °C typically used in thermal validation.	[22]
	Coefficient of determination (R^2)	Measures proportion of variance captured by the model; $R^2 \geq 0.85$ indicates excellent predictive fit.	[21,26]
	Wilcoxon signed-rank test (p-value)	Assesses statistical equivalence between real and simulated values across scenarios ($p > 0.05$).	[21]
Operational feasibility (*generic*)	System latency (s)	Measures sensor-to-actuation delay (<0.5 s); full DT loop delay captured separately.	[21,27]
	Local-to-global accuracy ratio (*cross-scale*)	Evaluates spatial consistency between localised sensing and full-domain predictions.	[22,25]
	Operational range (*performance envelope*)	Represents stability of control performance under various thermal or occupancy loads.	[21,28]
	Cost efficiency (*deployment-specific*)	Captures relative deployment affordability, scalability, and system integration effort; interpreted as an initial deployment indicator rather than a full lifecycle cost measure.	[21,27]

responsive, scalable, and standard-compliant control in residential environments [21,22].

II. METHODOLOGY

A. CASE STUDY DESCRIPTION

The experimental evaluation was conducted at the Huddersfield Smart House, a modern two-bedroom duplex specifically designed to support advanced research in environmental control and occupant wellbeing. The building is configured to enable natural ventilation and uniform thermal distribution. It is equipped with real-time environmental sensors and integrated within a broader smart infrastructure that supports building and health-focused research.

Room 2, as illustrated in Fig. 2, served as the primary experimental space for DT evaluation and thermal control validation. The test zone was comprehensively equipped with sensor–actuator infrastructure to facilitate real-time environmental data acquisition and ventilation control under various operational modes.

- Fig. 2a shows the physical testbed at the Huddersfield Smart House. The circled window indicates the DT-monitored aperture, which was outfitted with an automated actuator allowing dynamic control over air exchange based on real-time feedback.
- Fig. 2b presents the BIM-based DT geometry. This virtual model mirrored the physical structure and layout of the house, ensuring accurate boundary condition definitions for CFD-based simulations.
- Fig. 2c visualizes a 3D cutaway view of the duplex, highlighting Room 2 and the location of the automated window actuator. This room was selected for its strategic placement and exposure, ideal for evaluating ventilation dynamics. Green arrows represent air movement direction, and the actuator module (blue arrow) denotes the aperture's controllable element.
- Fig. 2d displays the first-floor plan layout, explicitly marking Room 2 within the DT's active monitoring domain. The red-circled window identifies the aperture used for passive ventilation control, linking back to both the physical (2a) and virtual (2b–2c) domains.

The testbed reflected standard UK residential design, with double-glazed apertures and thermally insulated walls, which supports practical relevance but does not guarantee wider-scale applicability on its own. This setup enabled realistic assessment of the DT's predictive and control capabilities under both passive and hybrid ventilation scenarios.

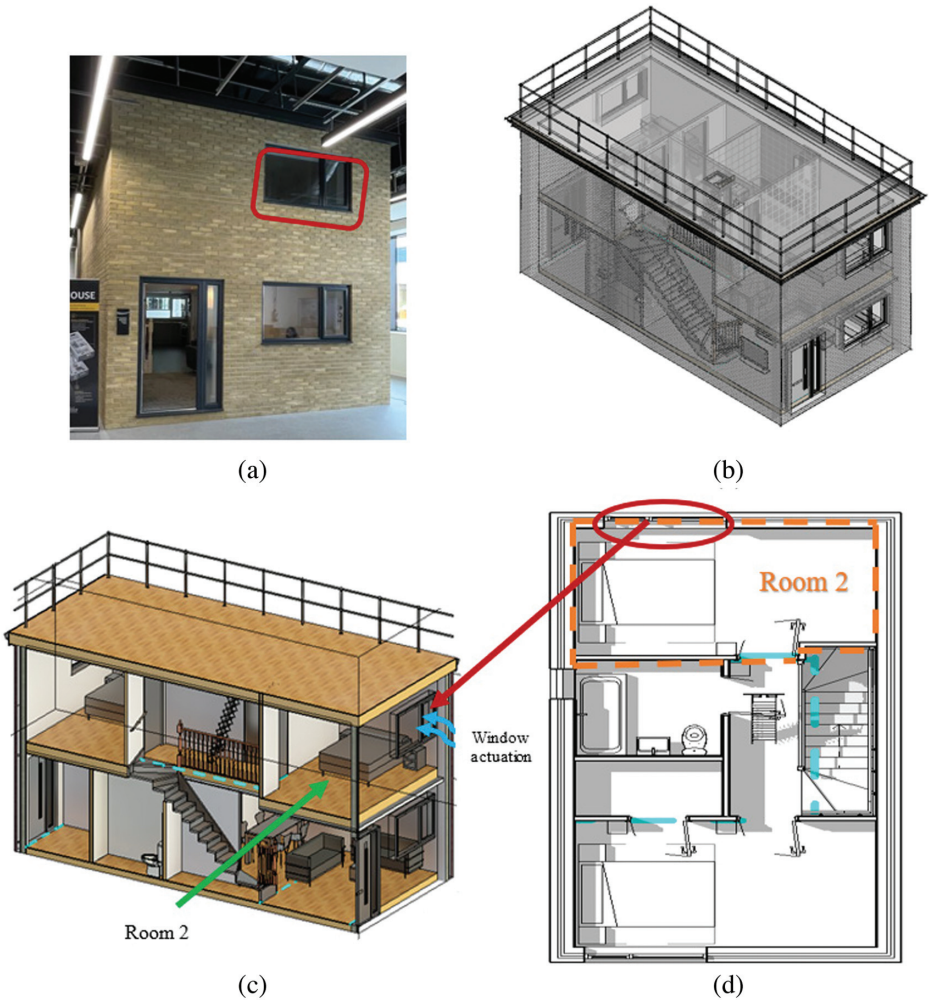

Fig. 2. Physical and virtual domains of the digital twin framework: (a) physical test environment (Huddersfield Smart House); (b) BIM-based digital geometry; (c) 3D model highlighting Room 2 with window actuation setup; and (d) first-floor plan view indicating the DT-monitored zone.

B. DT SYSTEM ARCHITECTURE FOR THERMAL COMFORT MANAGEMENT

The system architecture is founded on a real-time DT framework that ensures continuous synchronisation between the physical environment and its virtual counterpart. As illustrated in Fig. 3, the DT control architecture incorporates real-time sensing, wireless data transmission, and simulation-based optimisation to enable closed-loop regulation of smart window systems.

Window actuation is governed by programmable logic that interprets thermal indices such as PMV and PPD. These control decisions are computed locally using embedded control modules deployed at the sensor–actuator interface. This local processing approach eliminates the reliance on remote CPU-based interpretation, substantially reducing communication overhead and latency. As a result, control decisions are executed directly at the source of data generation, enabling rapid and decentralised actuation.

The overall architecture comprises three tightly integrated layers physical, cyber-physical, and cyber each contributing to the fulfillment of real-time performance goals associated with occupant thermal comfort and building energy efficiency.

The DT cyber layer is implemented using ANSYS Fluent for transient CFD simulation and MATLAB for KPI computation, supervisory optimisation and visualization, while ESP32 microcontrollers provide edge processing and actuator interfacing. Model reliability is maintained through BIM-derived room geometry and a hybrid poly-hexcore mesh (~3.41 million cells), with refinement in the high-gradient zones near the window opening and key thermal regions. The CFD model solves transient Reynolds-Averaged Navier–Stokes (RANS) with the standard k-ε turbulence closure to represent buoyancy-influenced indoor airflow and convective heat transfer under measured boundary conditions.

C. PHYSICAL LAYER SENSING – SENSING AND ACTUATION

Acting as the sensory interface, the physical layer (Fig. 4) comprises a distributed arrangement of sensors and actuators that facilitate bidirectional interaction between the physical environment and its digital counterpart. DHT22 hygrometer, MAX6675 thermocouples, MPX5010DP differential pressure sensors, and HC-SR04 ultrasonic modules collectively provide real-time data on air temperature, humidity, airflow, and window aperture. These data streams are essential for computing thermal comfort indices such as the PMV and PPD. Environmental control is executed via 12 V DC motors that dynamically adjust window openings in response to live measurements, aiming to maintain PMV within a tolerable band of ± 0.5. Data acquisition is managed by ESP32 microcontrollers, offering sub-second response with an end-to-end latency of approximately 0.2 seconds.

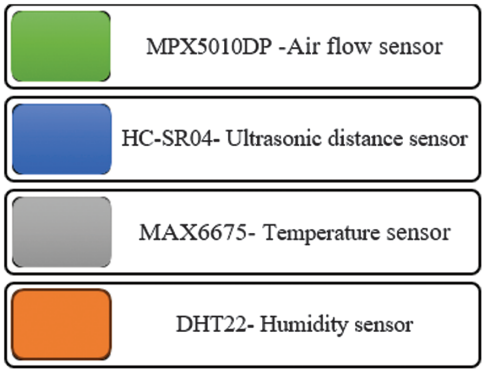

Fig. 4. Integrated sensor components for real-time monitoring in the digital twin physical environment.

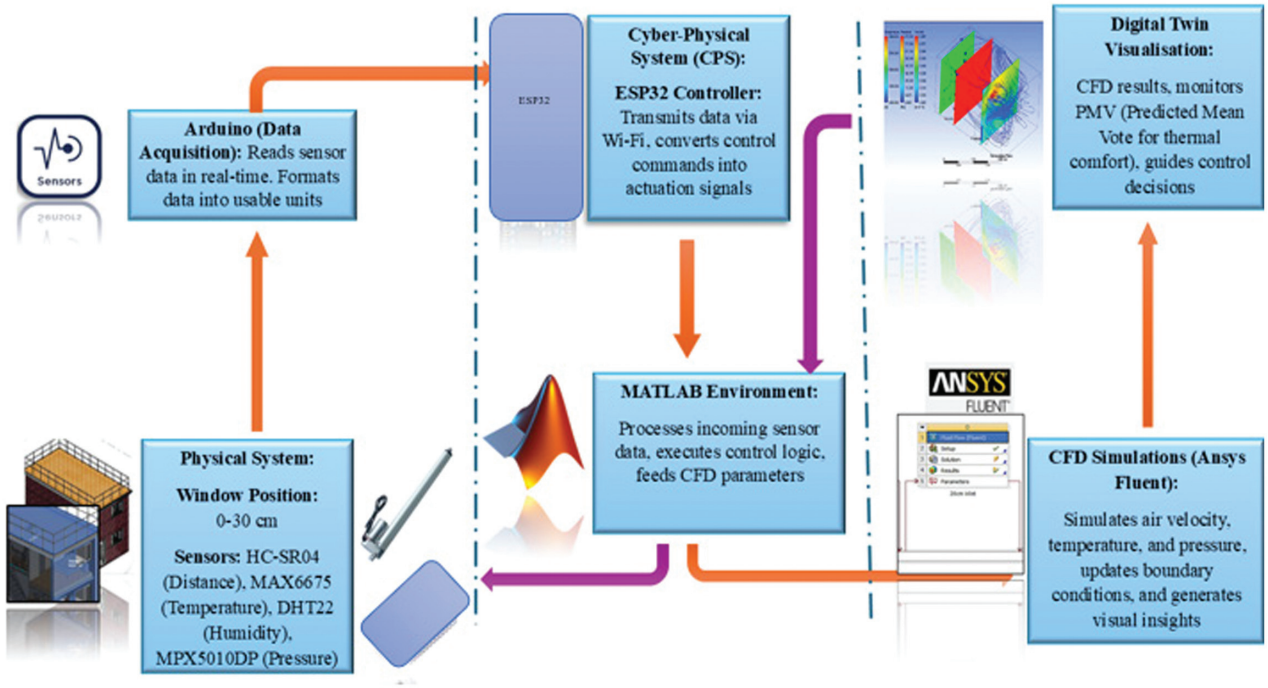

Fig. 3. Digital twin control architecture for adaptive smart window regulation.

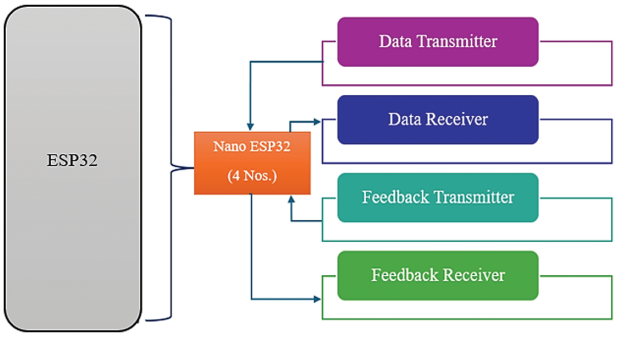

Fig. 5. Modular communication interface using nano ESP32 units for data exchange and feedback control.

D. CYBER-PHYSICAL LAYER – EDGE PROCESSING AND SECURE COMMUNICATION

As illustrated in Fig. 5, the cyber-physical layer bridges the sensing infrastructure with the control logic, leveraging a cluster of ESP32 modules for distributed computing. These microcontroller units execute preprocessing tasks, including outlier filtration (e.g., invalid humidity spikes), timestamp alignment, and drift compensation based on historical trends.

Synchronisation is handled at the edge before data is forwarded to the cyber layer. Each sensor packet is time-stamped, checked for missing values and obvious spikes, and then aligned within a short rolling time window so that temperature, humidity, airflow, and aperture measurements correspond to the same physical interval. Operational feasibility is evaluated using the end-to-end low-level latency from sensor acquisition to actuation, which is maintained at $\leq$5 s, ensuring that the actuation decision is based on the most recent validated measurements.

Encrypted Wi-Fi communication ensures data authenticity and resistance to external tampering. The communication stack maintains low-latency operation, achieving an average loop delay of 0.042 s adequate to preserve real-time synchronisation between ambient changes and system response.

E. CYBER LAYER – REAL-TIME SIMULATION AND PREDICTIVE CONTROL ARCHITECTURE

The cyber layer (Fig. 6) hosts the simulation and optimisation components underpinning intelligent decision-making. Transient CFD simulations, conducted in ANSYS Fluent, model spatial and temporal variations in airflow and thermal gradients, using boundary conditions updated per complete replica cycle (~6–7 minutes) based on aggregated live sensor data.

For each replica cycle, the edge-processed sensor bundle is mapped into CFD boundary inputs. Inlet air temperature, relative humidity (RH), and inlet velocity are updated from the corresponding sensors, while internal thermal conditions are applied using the parametric identifiers defined in the manuscript (e.g., named surfaces/zones and associated measured temperatures) to preserve physical-to-virtual consistency. The window-opening height is updated using the measured aperture gap and applied to the ventilation boundary representation for the current case. The CFD outputs are then sampled at defined probe locations to compute PMV/PPD and the validation KPIs, and the next supervisory decision is generated and passed to the edge device for actuation.

Each CFD replica cycle in this study starts from a fresh initialization rather than warm-starting from the previous converged field. This choice improves repeatability and avoids solution carry-over when boundary conditions

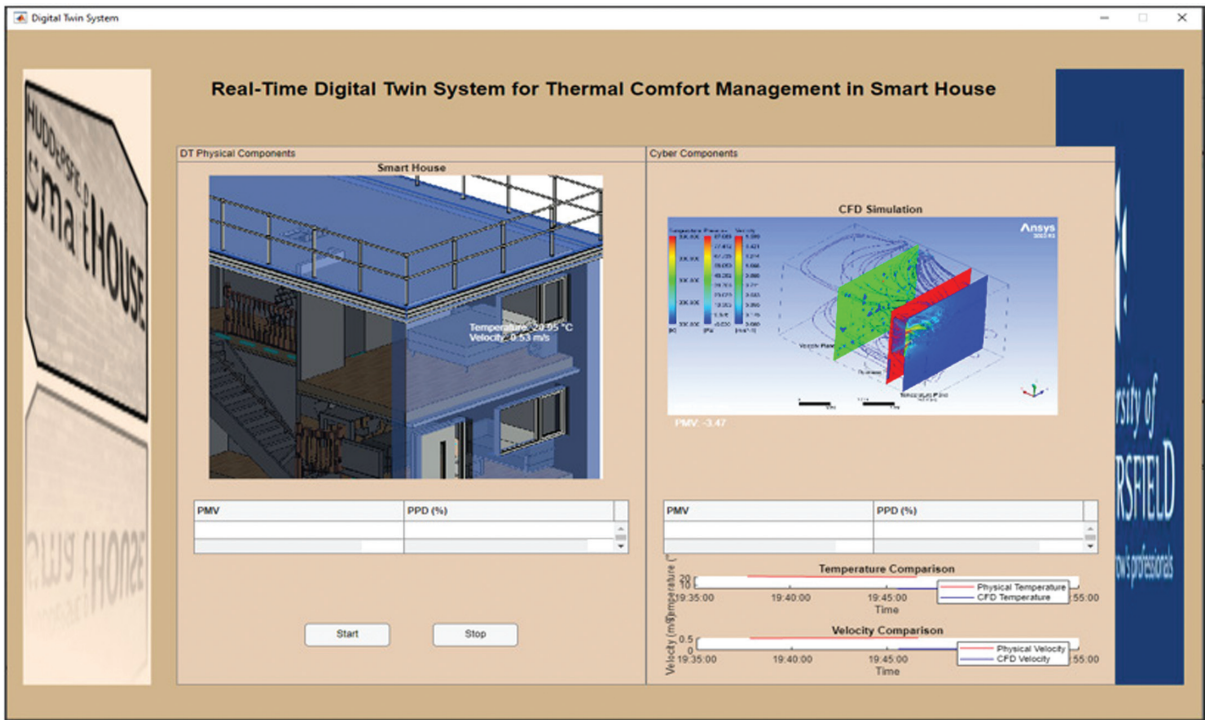

Fig. 6. Real-time digital twin dashboard linking smart house data acquisition with virtual simulation outputs.

change between test cases, but it increases the computational overhead of each update cycle. This is reflected in the reported full DT loop time and motivates future work on warm-start strategies to reduce refresh time while maintaining stability.

Control and optimisation logic. The control strategy is implemented in two layers to match the platform timing: a fast edge rule provides immediate comfort holding, while the cyber layer provides supervisory optimisation using CFD predictions. The edge rule operates on the most recent validated sensor bundle and applies a bound update to the window opening to keep comfort within a target band (PMV within ± 0.5). This layer is designed for operational feasibility and uses the measured low-level timing constraint (≤ 5 s from sensor acquisition to actuation) to ensure decisions are based on near-real-time room conditions.

In parallel, the cyber layer generates a supervisory recommendation using predicted comfort from the CFD model. The decision variable is the next window opening h_{k+1} (or equivalently the increment $\Delta h = h_{k+1} - h_k$). In this study, the actuator is commanded in discrete aperture states $h \in \{0,0.1,0.2,0.3\}$ m, which is consistent with the experimental scenarios; therefore, the admissible step is bounded by $|\Delta h| \leq 0.1$m and the physical range is $0 \leq h \leq 0.3$ m. The optimisation aims to reduce predicted discomfort while avoiding unnecessary actuation, using a quadratic objective of the form

$$\min_{\Delta h} (PMV_{k+1} - PMV_{target})^2 + \lambda(\Delta h)^2$$

subject to $h_{k+1} \in \{0,0.1,0.2,0.3\}$ m and $|\Delta h| \leq 0.1$m. The supervisory recommendation is updated at the DT replica cycle time, while the edge rule remains active to maintain comfort between CFD updates. This layered design separates rapid actuation (seconds) from prediction (minutes), which reflects the measured latency of the platform and improves practical deployability.

F. OPERATIONAL WORKFLOW INTEGRATION

As shown in Fig. 7, the DT control logic was implemented through a closed-loop architecture that integrates real-time sensing, simulation modelling, optimisation routines, and system visualization enabling adaptive and intelligent regulation of indoor environmental conditions. The workflow commences with sensor data acquisition, where environmental parameters such as temperature, humidity, airflow, and window position are captured through a cyber-physical interface. This raw data is then routed to a data translation and preprocessing unit, where signal conditioning and feature extraction are applied to convert the inputs into structured formats suitable for model-based simulation and control execution.

The preprocessed data is subsequently input into a CFD simulation module, developed in ANSYS Fluent, which conducts physics-based modelling of thermal and airflow dynamics within the indoor space. These simulations are continuously updated using live-streamed sensor data, ensuring that the evolving boundary conditions are accurately mirrored in the virtual environment. Outputs from the CFD simulations are channeled into an optimisation module, developed in MATLAB, which executes

Fig 7. Workflow of the digital twin system linking data, simulation, and control loops.

pre-programmed control logic to compute key thermal comfort indicators, namely the PMV and PPD. These metrics are derived from real-time computations based on centralised localised environmental variables such as temperature, humidity, and air velocity. A multi-objective control algorithm then determines the optimal response strategy, dynamically adjusting ventilation via motorised actuation to maintain comfort targets within acceptable bounds.

A dedicated graphical user interface (GUI), also developed in MATLAB, facilitates real-time monitoring, provides visual feedback, and allows manual override where necessary. The overall system performance is continuously assessed by comparing live sensor inputs against predefined comfort thresholds, thereby supporting robust thermal comfort management and operational efficiency.

G. REAL-TIME CONTROL LOGIC

Real-time reactive control of window apertures for maintaining indoor thermal comfort was achieved through an embedded logic program deployed on an IoT-based microcontroller. This microcontroller simultaneously transmits control commands to a motorised actuator. Computation of thermal comfort metrics PMV and PPD occur on the cyber layer and is wirelessly communicated to the actuation layer via a network of designated wireless transmitters (TX) and receivers (RX), each assigned unique identifier addresses to facilitate precise control routing.

These identifier mappings are embedded within the microcontroller's program script, allowing targeted delivery of computed PMV/PPD metrics from the CPU (cyber server) to the specific physical actuator unit. Upon receiving these metrics, the actuator interprets the data and executes the corresponding control logic, adjusting the window aperture to preserve or restore thermal equilibrium.

The logical interpretation scripted into the joint receiver and actuation controller is summarised in Table II.

This iterative cycle of 'monitor-analyse-optimise-adjust' (Fig. 8) ensured continuous compliance with predefined KPIs related to thermal comfort, energy efficiency, and operational reliability, thereby establishing a highly responsive and resilient DT-controlled thermal management system.

H. CFD MODEL SIMULATION

1). GOVERNING EQUATION. CFD simulations were performed using ANSYS Fluent, a robust solver widely applied in indoor environmental analysis. The simulations employed transient RANS equations, which effectively captured unsteady airflow and convective heat transfer within the Huddersfield Smart House domain [29]. The governing equations applied in the CFD model were as follows:

1. Continuity Equation:

$$\nabla \cdot (\rho u) = 0$$

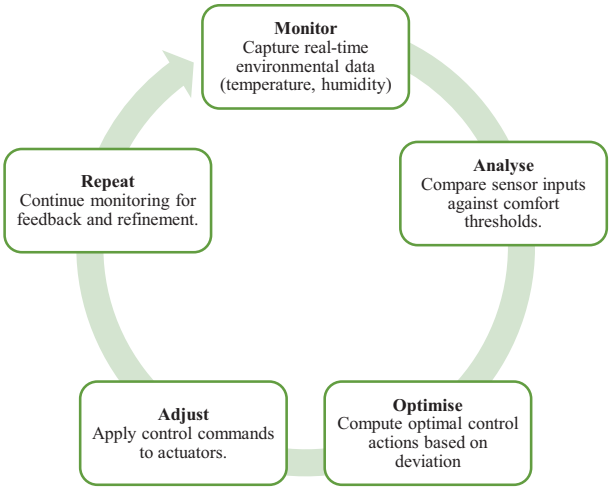

Fig. 8. Feedback control logic flow for dynamic adjustment in digital twin systems.

2. Momentum Equation (Navier–Stokes)

$$\rho(u \cdot \nabla)u = -\nabla p + \mu \nabla^2 u + \rho g$$

3. Energy Equation

$$\rho c_p (u \cdot \nabla T) = k \nabla^2 T + S_T$$

These equations form the fundamental basis for predicting realistic airflow and thermal distributions crucial for accurate thermal comfort analyses.

2). BOUNDARY CONDITIONS AND SIMULATION DOMAIN. Boundary conditions were explicitly defined to accommodate dynamic, real-time environmental inputs streamed live. Inlet conditions were set and updated in real time using sensor-derived data streams, including air temperature (MAX6675), ambient RH (DHT22), air velocity (MPX-5010DP), and aperture gap measurements (HC-SR04) recorded at the base of the window opening.

Pressure boundary conditions at vents and other openings were assigned atmospheric references to accurately model buoyancy-driven airflow within the indoor space [30]. Thermal boundary conditions for the floor, ceiling, and walls were configured using calibrated thermocouples (MAX6675 K-type), providing precise, real-time measurements of conductive and convective heat exchange across internal surfaces. These configurations enabled accurate and current thermal resolution, ensuring reliability in simulating transient thermal behavior within the environment.

The simulation domain itself was dynamically updated based on real-time inputs from the adjustable aperture gap. These inputs, interpreted via embedded control logic, enabled accurate and responsive adaptation of the

Table II. Logical control actions based on PMV thresholds for actuation and thermal comfort interpretation

Received metric	Action taken by controller	Resulting interpretation
$PMV \leq -0.5$	Retract actuator arm for 5 seconds	Indoor reference temperature is too low; the room is cold or chilly.
$-0.5 < PMV < 0.5$	Maintain current state; no action taken	Indoor thermal conditions are optimal for occupant comfort.
$PMV \geq 0.5$	Extend actuator arm for 5 seconds	Indoor reference temperature is high; increase ventilation.

simulation boundary in line with passive ventilation conditions, thereby achieving high-resolution, real-time environmental modelling.

3). MESHING AND TURBULENCE MODELLING. A hybrid poly-hexcore mesh containing approximately 3.41 million elements was generated to optimize simulation accuracy and computational load as shown in Fig. 9. Structured grids were applied around heating and ventilation domain inlets, apertures, and high-gradient thermal zones to ensure resolution of local phenomena. Unstructured grids were used in regions with lower flow variability to reduce processing overhead [31].

The standard k-ε turbulence model was adopted for its well-established performance in indoor airflow simulation, offering a balance between convergence speed and prediction reliability. It was particularly suitable for simulating buoyancy-influenced ventilation scenarios and enabled integration with real-time DT control logic [32].

I. DIGITAL TWINS OPERATION OF WINDOW

The DT integrated IoT sensing, CFD simulation, and adaptive control across four window-opening configurations (0 m, 0.1 m, 0.2 m, and 0.3 m).

The DTs functional loop operates across three tightly coupled phases:

- State Detection: Real-time sensor-based identification of physical window position and environmental conditions.
- Virtual Replication: High-resolution CFD simulations of detected physical states.
- CFD-Driven Actuation: Optimal control decisions calculated to ensure comfort and energy efficiency.

1). DETECTION AND VIRTUAL REPLICATION. Accurate modelling and temporal analysis of interactions within the indoor environment were realised through a validated approach comprising systematic 'detection' and 'sampling' of spatio-temporal boundary states. This process was underpinned using high-resolution IoT-enabled thermal sensors (MAX6675 with ESP32) to capture the thermal characteristics of building surfaces (walls, ceiling, floor, heat sources, and sinks). These sensor readings were transmitted and mapped into the CFD model.

At boundary inlets, primarily at the smart window aperture, ambient airflow characteristics were similarly recorded in real time to enable accurate simulation of ventilation-induced thermal effects. The inlet velocity and environmental conditions of emerging airflow were dynamically recorded and integrated into the model (see Section 3.8.1).

Table III. Sensor positions and corresponding parametric identifiers for CFD boundary assignment

Sensor position (indoor room)	Parametric ID (CFD)
MPX5010DP (velocity – inlet)	P1
MAX6675 (Temperature – inlet)	P2
DHT22 (Rel. Humidity – inlet)	P3
MAX6675 (Temperature – ceiling)	P4
MAX6675 (Temperature – floor)	P5
MAX6675 (Temperature – wall north)	P6
MAX6675 (Temperature – wall west)	P7
MAX6675 (Temperature – wall west-extension)	P8
MAX6675 (Temperature – wall south)	P9
MAX6675 (Temperature – wall south-extension)	P10
MAX6675 (Temperature – wall east)	P11
MAX6675 (Temperature – sources)	P12
MAX6675 (Temperature – sinks)	P13

The full room domain was replicated within the CFD model using a refined CAD geometry that accurately represented the physical room configuration. Boundary conditions for all modeled surfaces were defined by assigning corresponding thermal properties in the simulation environment.

Each parameter in the CFD model was assigned a unique identifier (e.g., P1, P2, P3 . . .), with real-time thermal sensor values accurately mapped to their respective zones. For instance, temperature readings from the MAX6675 sensor mounted on the west wall were mapped to 'P6' in the simulation model. This value, expressed in Kelvin (K), directly governed the thermal input condition for that wall surface. Such parametric assignments were applied across all zones, ensuring faithful physical-to-virtual representation of thermal dynamics within the indoor space. The sensor positions and corresponding parametric identifiers used for CFD boundary assignment are summarised in Table III.

The aperture gap, measured by HC-SR04 ultrasonic sensors, was dynamically transmitted into MATLAB via embedded script logic. This automated process triggered real-time CFD case updates (see Figs. 10a, 11a, 12a, 13a),

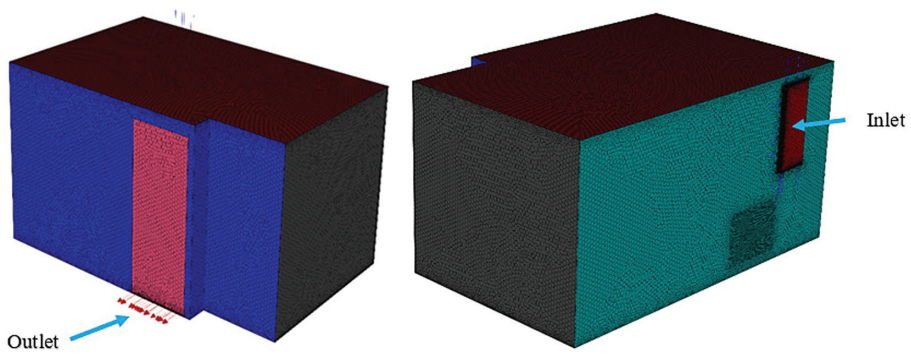

Fig. 9. Poly-hexcore mesh configuration for CFD simulation of the smart house case study.

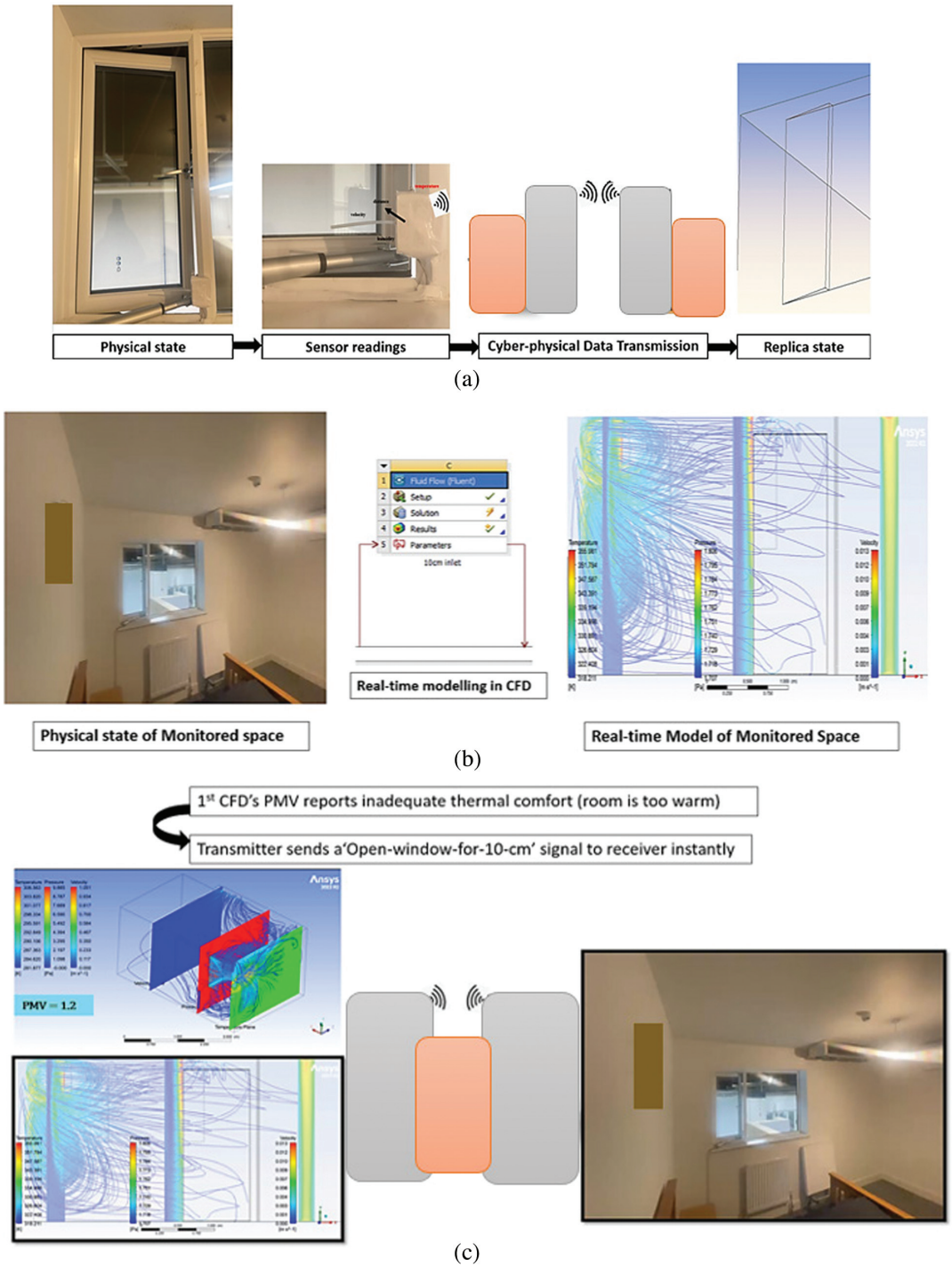

Fig. 10 (a) Real-time sensing and CFD translation (0.1 m). (b) Real-time replication of physical state (0.1 m). (c) CFD analysis and control action execution (0.1 m).

facilitating minimal latency in synchronising simulation steps with the evolving indoor environment.

Complementary airflow and humidity data from DHT22 sensors further reinforced model reliability (Fig 10b–13b). For example, a 0.3 m aperture setting (Fig. 12b) yielded simulated velocities ranging from 0.2 to 1.5 m/s near window frames, closely matching measured values. Similarly, the 0.2 m aperture configuration (Fig. 11b) produced thermal profiles between 19.85°C and 24.85°C, in strong agreement with MAX6675 readings. These results, obtained from transient RANS simulations in ANSYS Fluent, exhibited prediction errors under 2%, demonstrating high accuracy and consistent virtual-physical alignment.

2). ADAPTIVE CONTROL OF THE DIGITAL TWINS. The adaptive window control strategy was driven by CFD simulation outputs, enabling dynamic responses to real-time environmental states:

- 0.1 m Opening (Fig. 10c): The real-time DT simulation identified inadequate thermal comfort, registering a PMV of 2.1 indicative of elevated indoor temperatures.

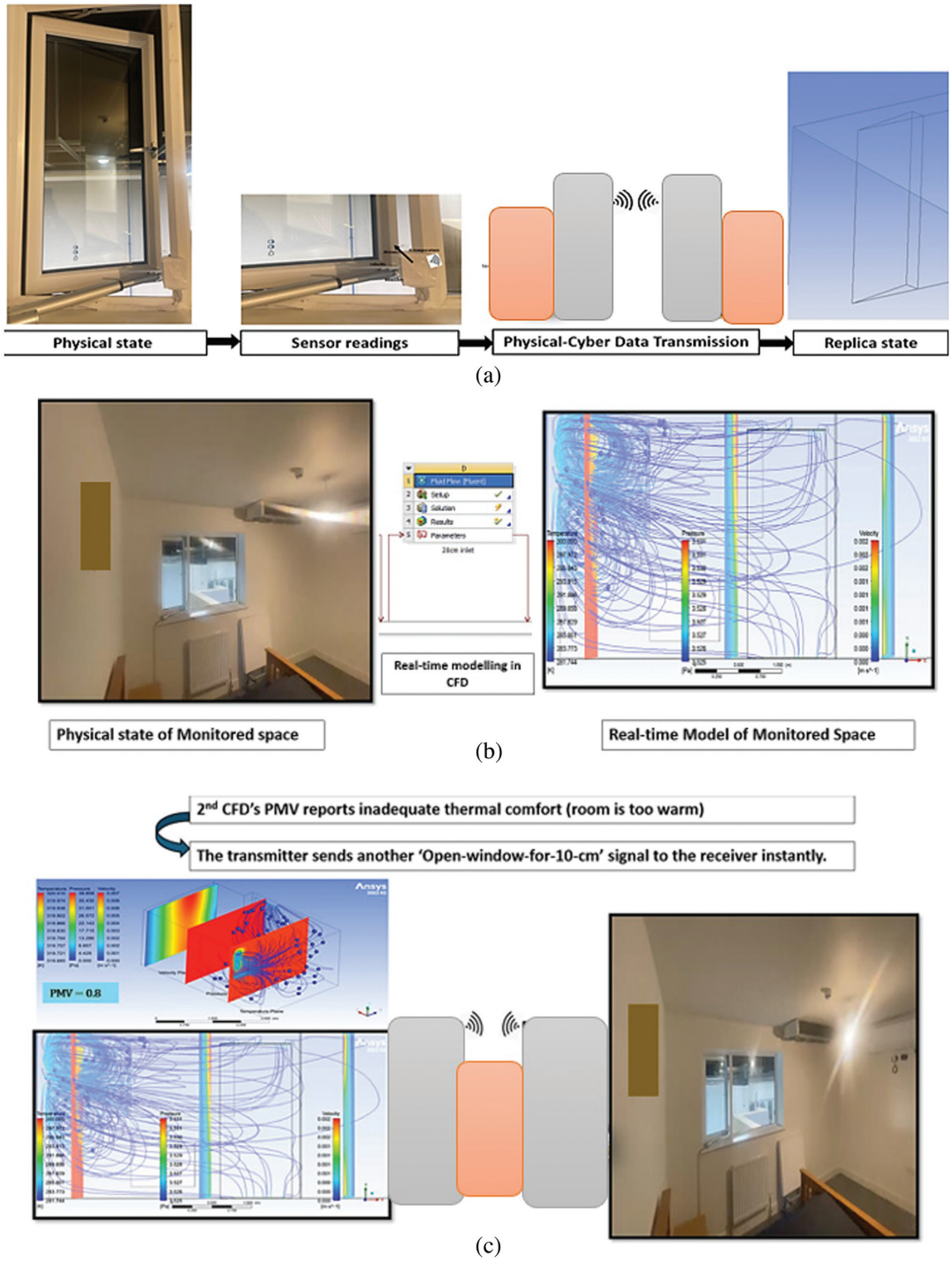

Fig. 11 (a) Real-time sensing and CFD translation (0.2 m). (b) Real-time replication of physical state (0.2 m). (c) CFD analysis and control action execution (0.2 m).

This thermal deviation triggered a control response from the embedded microcontroller, which extended the window aperture by 0.1 m to facilitate passive cooling. Simultaneous physical sensor readings corroborated the model's prediction, recording a PMV of 2.39. However, the system also detected constrained airflow velocity, indicating limited ventilation effectiveness at this aperture.

- 0.2 m Opening (Fig. 11c): In this scenario, DT simulation continued to detect thermal discomfort, with a predicted PMV of 2.0. Consequently, the control logic issued a further command to increase the window aperture to 0.2 m. This incremental actuation resulted in a measured PMV of 2.03, signifying improved thermal regulation. CFD results further showed improved airflow distribution across space, enhancing energy efficiency. This aperture setting was particularly effective during peak occupancy, achieving up to 27% energy savings through improved airflow uniformity.

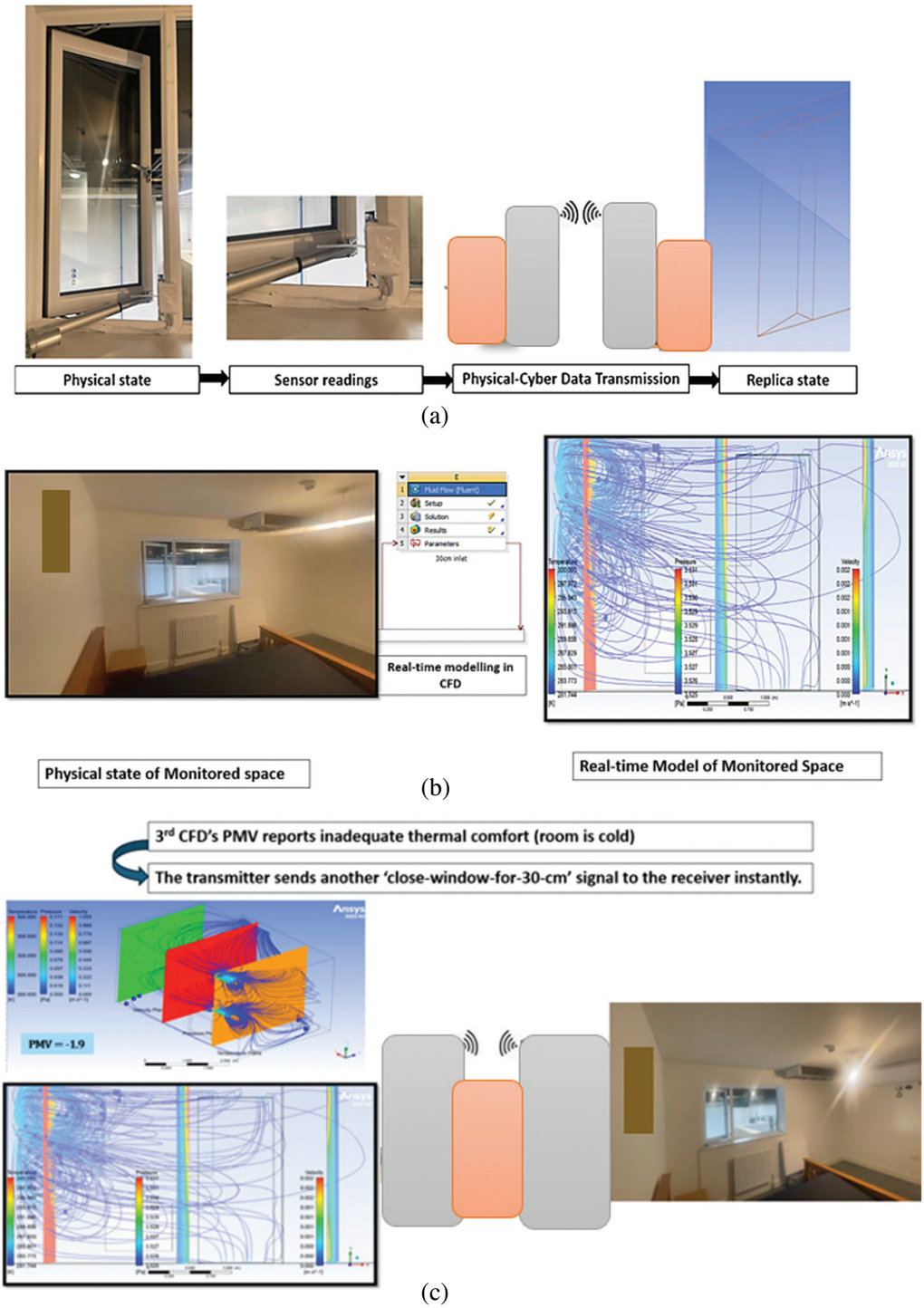

Fig. 12 (a) Real-time sensing and CFD translation (0.3 m). (b) Real-time replication of physical state (0.3 m). (c) CFD analysis and control action execution (0.3 m).

- 0.3 m Opening (Fig. 12c): At this stage, the DT system detected excessive cooling losses, with internal temperatures dropping below the lower comfort threshold (≥24 °C). In response, the controller closed the aperture completely, returning to a 0.0 m setting to prevent over-ventilation and restore thermal comfort.
- 0.0 m Opening (Fig. 13c): During idle states, the DT simulation confirmed that the sealed window condition maintained PMV/PPD values within ISO 7730 comfort thresholds. This validated the appropriateness of keeping the aperture closed to conserve energy without compromising comfort.

Across all tested conditions, the adaptive control strategy consistently prioritized occupant comfort during active occupancy and optimized energy savings during unoccupied periods. This intelligent regulation loop validates the DT system's ability to dynamically balance energy consumption and indoor environmental quality through real-time sensing, simulation, and actuation.

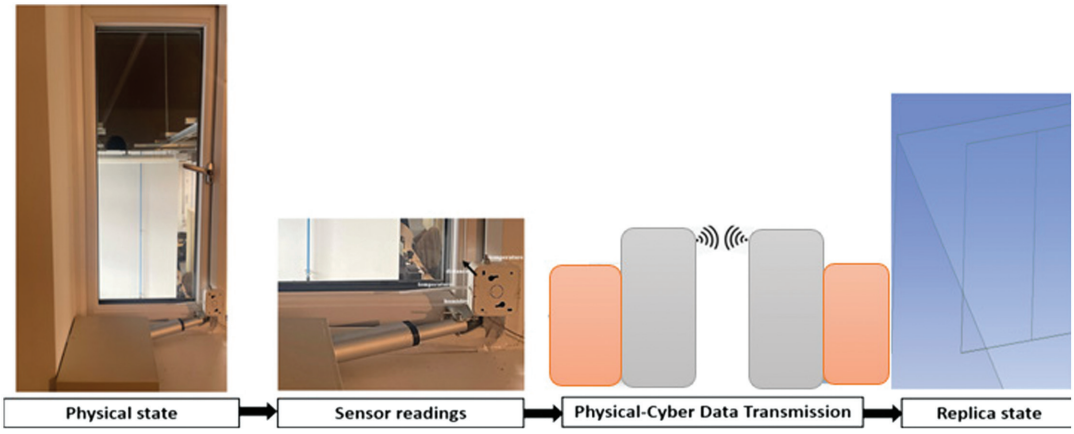

(a)

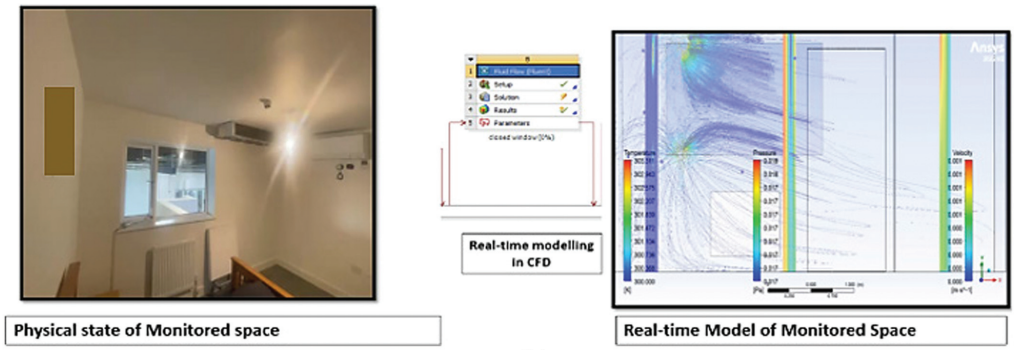

(b)

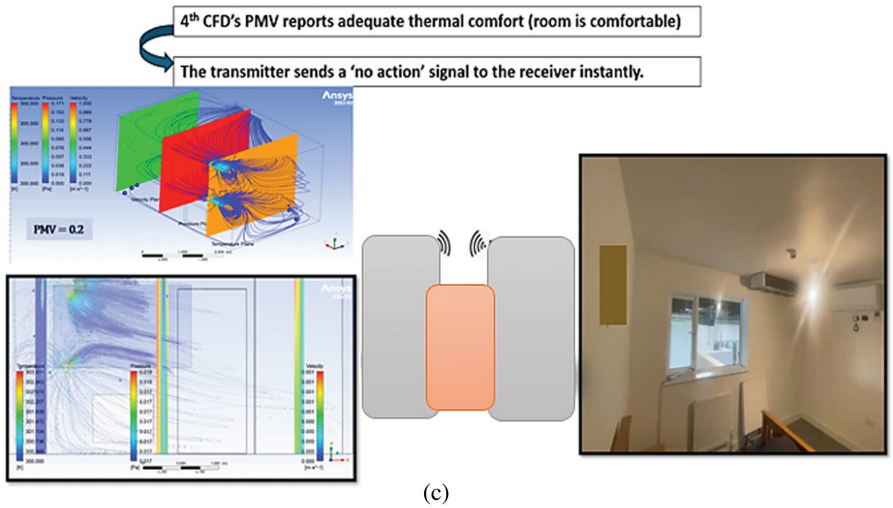

(c)

Fig. 13 (a) Real-time sensing and CFD translation (0 m). (b) Real-time replication of physical state (0 m). (c) CFD analysis and decision execution (0 m).

3). REAL-TIME SYNCHRONISATION. The DT system exhibited consistent synchronisation performance throughout the closed-loop thermal control cycle, seamlessly integrating CFD, sensor data processing, and mechanical actuation. Wireless transmission of environmental sensor data introduced negligible delay (~0.2 seconds); however, the complete cycle from simulation initiation to actuation response required approximately 6–7 minutes per full session, encompassing 20 iterative updates. This timeframe reflects the entirety of internal DT operations, including CFD convergence, thermal comfort assessment via PMV/PPD, and embedded actuation command execution.

During a representative scenario involving a step change in aperture size from 0.1 m to 0.2 m, the DT recorded a mean physical actuation delay of 3.2 seconds, with less than 1.5% deviation between sensor feedback and CFD-predicted values (Figs. 12c–15c). While this duration includes broader replica iterations intended for validation, the core actuation logic responded swiftly enough to maintain thermal stability and support adaptive window regulation.

On balance, the DT framework upheld high synchronisation precision, enabling timely adaptation to fluctuating indoor conditions. These findings underline its practical potential for real-world thermal management systems demanding continuous comfort, energy-aware performance, and minimal latency.

4). BASELINE SENSOR-ONLY RULE-BASED CONTROLLER. In addition to the DT workflow, a baseline controller was defined as a reference for comparison. The baseline is sensor-only and rule-based, with no CFD model and no prediction. At each decision point, it uses the latest sensor readings (temperature and RH, and where available a representative indoor air speed) and applies a fixed threshold rule to select the next discrete window-opening state. The window actuator is commanded only in the discrete aperture states used in the experiments, $h\epsilon\{0,0.1,0.2,0.3\}$m. If the measured (or sensor-derived) comfort estimate indicates the room is too warm (above the comfort band), the baseline steps the window to the next larger opening; if it indicates the room is too cool (below the band), it steps to the next smaller opening; otherwise, it holds the current opening. This baseline therefore represents a fast, reactive

Table IV. Quantitative comparison of observed indoor conditions and digital twin (DT) predictions across heating and ventilation regimes

Window opening	Operating mode	Observed indoor dynamics	DT prediction	Interpretation and comments
0 m (sealed)	Heated	Temperature increased sharply, peaking at 33.4 °C; relative humidity (RH) decreased substantially to 21%. Thermal discomfort significantly intensified, with PMV rising from 1.34 to 2.39 and PPD escalating from 47% to 84%.	DT predictions indicated a systematic cool-dry bias, remaining 0.5–1.0 °C cooler and approximately 1% RH lower than measured values. Comfort indices predicted slightly lower discomfort (PMV $\leq$ 0.3 lower, PPD $\leq$ 4% lower).	Observed biases attributed to minor latency in the virtual response; overall trends effectively captured.
	Non-heated	Conditions remained stable around 23.6 °C and 32% RH. Thermal comfort indices remained neutral (PMV $\approx$ 0, PPD $\approx$ 5%).	DT predictions matched sensor data with negligible deviations, well within sensor resolution limits.	Validates accuracy of the CFD and energy-balance models in passive conditions without thermal interventions.
0.1 m	Heated	Peak indoor temperature reached 33.4 °C, while RH dropped from 24.5% to 21%. PMV stabilized at a discomforting level (2.39).	DT's temperature and RH biases were significantly reduced compared to the sealed scenario ($\leq$0.6 °C and $\leq$1% RH, respectively). Comfort indices closely aligned with observations.	Demonstrates accurate representation of mixed-mode ventilation; partial ventilation effectively moderated heating intensity and ventilation losses cycling.
	Non-heated	Conditions similar to sealed scenario but consistently warmer by approximately 0.2 °C. Comfort indices maintained stable, neutral conditions.	DT predictions closely tracked actual measurements, showing sub-degree accuracy. Comfort indices closely overlapped sensor readings.	Validates accuracy of the natural ventilation algorithm, even at minimal apertures.
0.2 m	Heated	Peak temperature moderated to 32.4 °C, RH reduced to 19%, and PMV capped at 2.03, indicating improved but still high thermal discomfort.	DT maintained high accuracy, with temperature error below 0.4 °C, RH differences within approximately 1%, and PMV within $\leq$ 0.15 of measured values.	Affirms DT's capability to accurately simulate balanced hybrid ventilation, ensuring reliable predictions during moderate ventilation conditions.
	Non-heated	Morning airflow briefly lowered room temperature to approximately 23.3 °C, then gradually warmed through the day.	DT exhibited minor warm bias (~0.5 °C) during morning hours but closely matched measurements thereafter, showing strong overall alignment.	Suggests minor adjustments to solar-gain parameters for improved transient condition accuracy; validates general predictive robustness.
0.3 m	Heated	Natural ventilation dominant regime: temperature peaked at 32.3 °C, humidity stabilized at 18.9%, PMV reached 2.00, and PPD was high at 66%.	DT achieved excellent predictive accuracy, closely following sensor measurements (temperature deviation $\leq$0.4 °C, RH within 1%). Comfort metrics (PMV/PPD) differed minimally ($\leq$0.2 PMV and $\leq$3% PPD).	High model reliability maintained even under strong natural ventilation and minimal thermal intervention influence, supporting DT's across dynamic ventilation scenarios.
	Non-heated	Temperature initially rose to 26.3 °C during morning, decreasing steadily to 22.8 °C by afternoon; humidity stabilized around 31%, PMV gradually transitioned from neutral (0.05) to slightly cool (−0.2).	DT predictions initially cooler by approximately 0.5 °C but converged closely by afternoon; comfort indices aligned well with actual measurements.	Confirms DT's capability to accurately model buoyancy-driven airflow and temperature exchange without thermal intervention, highlighting reliable performance in passive operation modes.

strategy that relies on current measurements only, and it ignores spatial airflow distribution, spatial comfort gradients, and the effect of the opening on future states.

J. VALIDATION AND COMPARATIVE ANALYSIS

The DT framework was validated across four window aperture configurations (0, 0.1, 0.2, and 0.3 m) under dynamic heating and ventilation conditions. Validation metrics included indoor air temperature, RH, and thermal comfort indices PMV and PPD benchmarked against real-time sensor data. Under sealed, heated conditions (0 m), the DT slightly underestimated peak temperatures by 0.5–1.0 °C and RH by ≈1%, attributed to minor lag in simulated heating and ventilation actuation. PMV and PPD deviations remained within acceptable thresholds, indicating minimal perceptual impact. At 0.1 m aperture, prediction errors were halved, demonstrating improved accuracy under hybrid ventilation conditions. For 0.2 m openings, representing balanced mechanical-natural ventilation, temperature errors remained below 0.4 °C and RH discrepancies within 1%, confirming the DT's dependability in modelling transitional flow regimes. At 0.3 m, where buoyancy-driven ventilation prevailed, DT outputs closely aligned with physical measurements, with deviations consistently within 0.4 °C for temperature and 1% for RH. Across all scenarios, PMV and PPD errors remained within ISO 7730 interpretive limits (± 0.2 PMV, ± 5% PPD), validating the DT's reliability in delivering occupant-centric comfort assessments under dynamic thermal conditions.

K. QUANTITATIVE EVALUATION OF THE DIGITAL TWINS

1). KPI CATEGORY. A structured, multi-layered evaluation protocol was implemented to quantify the performance of the DT across four key domains: thermal comfort, energy efficiency, system reliability, and operational feasibility. This protocol integrates deterministic error metrics, statistical significance testing, and cost–benefit analysis to holistically assess predictive accuracy, control efficiency, and deployment viability. The KPIs, their governing equations, and compliance thresholds are summarized in Table V, with detailed rationale provided below.

2). KPI DEFINITIONS AND THRESHOLDS. Thermal comfort was evaluated using the ISO 7730 six-factor model for PMV and its derivative PPD. Compliance thresholds were set at MAE ≤ 0.15 for PMV and MAE ≤ 10% for PPD, adhering to ISO Class A criteria. Energy efficiency was quantified as the percentage reduction in thermal and ventilation energy consumption relative to a baseline rule-based controller, with a target of positive savings (>0%). System reliability was assessed through MAE, RMSE (≤ 2.0°C), and coefficient of determination (R^2 ≥0.85), complemented by a non-parametric Wilcoxon signed-rank test ($p > 0.05$) to verify statistical equivalence between physical and simulated data. For variance-gated reporting, the minimum variance threshold σ_{min} is set based on the sensor resolution and practical noise floor already used in this study (e.g., ±0.5 °C for DHT22 temperature normalisation and the RH tolerance benchmark used for local-to-global normalisation), so that correlation metrics

Table V. KPI definitions and validation criteria

KPI category	Performance indicator	Governing expression	Compliance threshold*
Thermal comfort	Predicted Mean Vote (PMV)	ISO 7730 six-factor model	MAE ≤ 0.15
	Predicted Percentage Dissatisfied (PPD)	$100 - 95e^{-0.03353\mathrm{PMV}^4 - 0.2179\mathrm{PMV}^2}$	MAE ≤ 10
Energy efficiency	Thermal and ventilation energy saving (%)	$\mathrm{Saving} = \frac{(E_{\mathrm{baseline}} - E_{\mathrm{DT}})}{E_{\mathrm{baseline}}} \times 100$	> 0 (positive saving)
System reliability	Mean absolute error (MAE)	$\mathrm{MAE} = \frac{1}{n}\sum_{i=1}^{n} \lvert y_{\mathrm{physical},i} - y_{\mathrm{simulated},i} \rvert$	–
	Root mean square error (RMSE)	$\mathrm{RMSE} = \sqrt{\frac{1}{n}\sum_{i=1}^{n} (y_{\mathrm{physical},i} - y_{\mathrm{simulated},i})^2}$	RMSE ≤ 2.0°C
	Coefficient of determination (R^2)	$R^2 = 1 - \frac{\sum_{i=1}^{n} (y_{\mathrm{physical},i} - y_{\mathrm{simulated},i})^2}{\sum_{1=1}^{n} (y_{\mathrm{physical},i} - \bar{y}_{\mathrm{physical},i})^2}$	R^2 ≥0.85 (reported and interpreted only when measured variance is above sensor noise floor; otherwise MAE and RMSE are primary)
	Wilcoxon signed-rank (p-value)	$\mathrm{Rank} - \mathrm{sum\ test\ on\ d}_i = y_i^{\mathrm{phys}} - y_i^{\mathrm{sim}}$	$p > 0.05$ (non-significant)
Operational feasibility	System latency (s)	• Sensor–actuator latency: $t_{lat} = t_{actuation} - t_{aquisition}$ • DT full-loop latency: $t_{DT-loop} \approx 6 - 7$ min	$t_{lat} \leq 5$s Simulation+DT cycle
	Local-to-global accuracy ratio	$\mathrm{Ratio} = \frac{\mathrm{RMSE_{DT}}}{\sigma_{\mathrm{sensor}}}$	Ratio ≤ 1
	Operational range	Domain where RMSE ≤ 2°C; $R^2 \geq 0.85$ applied only in dynamic segments that pass the variance gate	-
	Cost efficiency	$\mathrm{CE} = \frac{\mathrm{Energy\ saving}(\%)}{\mathrm{Deployment\ cost}(£)}$	Higher CE = better deployment return

are interpreted only when the measured signal contains meaningful dynamics above measurement noise.

Operational feasibility metrics included low-level latency (≤ 5 s) from sensor acquisition to actuation, reflecting responsiveness at the hardware–control interface. In contrast, the full DT control loop including CFD convergence, PMV/PPD evaluation, and actuation decision-making averaged 6–7 minutes per complete update cycle. Additional feasibility indicators comprised the local-to-global accuracy ratio ($\text{RMSE}/\sigma_{\text{sensor}} \leq 1$) and operational range ($\text{RMSE} \leq 2°\text{C}$ and $R^2 \geq 0.85$ applied only in dynamic segments that pass the variance gate).

CE was expressed as annualized thermal energy savings per unit deployment cost, where higher ratios indicate improved economic viability and system affordability.

The KPI thresholds were selected to be practical for a residential DT that relies on low-cost sensing, spatially varying indoor fields, and short monitoring windows. $\text{RMSE} \leq 2.0°\text{C}$ is used as a reliability bound to limit absolute temperature error under realistic indoor gradients near openings and heat sources. In this study, comfort indices (PMV/PPD) are treated as the primary compliance criteria because they directly represent occupant perception, while temperature and humidity errors provide supporting evidence of model agreement.

The coefficient of determination ($R^2 \geq 0.85$) is retained to describe tracking performance during dynamic periods (e.g., heating transients or aperture-driven transitions) where measured variance is sufficient. However, in near-steady conditions typical in homes, correlation metrics can become unstable and may appear low or negative even when absolute errors are small. This paper applies a variance-gated approach: when the standard deviation of the measured series is close to the sensor noise floor (as reflected by the sensor tolerances used in this study), MAE and RMSE are prioritized and R^2 is flagged as non-informative for that segment. [33].

3). ANALYSIS WORKFLOW. For each window-opening scenario (0–0.3 m), a structured analytical framework was implemented. First, time-synchronised physical measurements including dry-bulb temperature, RH, and ventilation-related energy use were aligned with corresponding DT outputs and tagged by operational mode. This assumption supports controlled comparison across scenarios, but it also limits generalizability because clothing level and metabolic activity vary between occupants and over time, which can shift PMV/PPD estimates under real residential use. PMV values were converted to PPD via Fanger's exponential relation, with errors evaluated against Table IV thresholds.

System reliability metrics were derived from paired physical-simulated datasets. MAE and RMSE quantified absolute errors for temperature and humidity, while R^2 assessed temporal correlation. A two-tailed Wilcoxon signed-rank test ($\alpha = 0.05$) was applied to residuals to determine statistical equivalence, with repeatability confirmed through three simulation runs using distinct random seeds. Energy performance was calculated by integrating thermal control power consumption over ten-hour cycles for both baseline and DT-controlled operations, with savings expressed as a percentage reduction relative to the baseline.

Operational feasibility metrics were extracted from system logs and error distributions. End-to-end latency defined as the interval between sensor acquisition and actuator acknowledgment was averaged across dynamic control cycles. Local-to-global accuracy ratios normalised RMSE against sensor tolerances (e.g., $\pm 0.5°\text{C}$ for DHT22 temperature sensors), while operational range compliance was mapped in RMSE-R^2 space. Finally, CE was computed as the ratio of annualized energy savings to total hardware deployment costs, providing a dimensionless metric for return on investment (Table IV).

III. RESULTS

This section reports statistical validation of the DT system across variable window apertures (0 m to 0.3 m) within Room 2 of the Huddersfield smart house. The assessment framework incorporates ISO 7730-derived thermal comfort indicators, model prediction accuracy, and system-level feasibility metrics to evaluate both reliability and readiness for autonomous deployment.

A. PMV & PPD COMPLIANCE TO ISO-7730

The DT framework demonstrated strong adherence to ISO 7730 thermal comfort standards. Across all eight operating points, PPD-MAE values remained below the 10% threshold, with no scenario exceeding 4%, thereby ensuring 100% compliance. PMV compliance was achieved in seven of eight configurations (88% pass rate), with MAE values ≤ 0.15 in all cases except Heated 0.1 m as shown in Fig. 14, where PMV-MAE reached 0.237. This deviation likely resulted from stratified airflow and ventilation actuation latency under partially sealed conditions.

Mixed-mode and passive ventilation regimes (0.2–0.3 m) consistently maintained PMV-MAE values within ISO Class A limits (0.08–0.117), confirming the system's suitability for ventilated low-energy settings. The non-heated 0 m scenario delivered the most accurate comfort prediction, with PMV-MAE of 0.073 and PPD-MAE of 0.25, underscoring the DT's precision in stable, passively regulated environments.

B. THERMAL COMFORT VARIABLES

In Fig. 15, thermal comfort analysis showed that PMV-MAE remained below the ISO 7730 threshold of 0.15 in 88% of cases (7 out of 8 scenarios), with only Heated 0.1 m exceeding the limit (PMV-MAE = 0.237). PPD-MAE values were uniformly compliant across all scenarios, remaining well below 10%, with the highest recorded error at 3.604 in the Heated 0 m condition.

Temperature and humidity deviations remained within acceptable sensor bounds (≤ 0.7 °C and $\leq 1\%$ RH) across all test points, except in the sealed Heated 0 m configuration where humidity MAE reached 1.137. In scenarios involving passive and hybrid ventilation (0.2–0.3 m apertures), the DT system effectively reduced overshoots in thermal and ventilation actuation during transition, sustaining PMV and PPD values within the ISO Class A thresholds. These outcomes highlight the model's robustness in maintaining occupant comfort across both steady-state and dynamic indoor conditions.

C. PREDICTIVE ACCURACY (R^2 CORRELATION)

The R^2 correlation analysis (Fig. 16) revealed stratified predictive accuracy across variables. PPD predictions consistently achieved $R^2 \geq 0.85$ in all heated and most non-

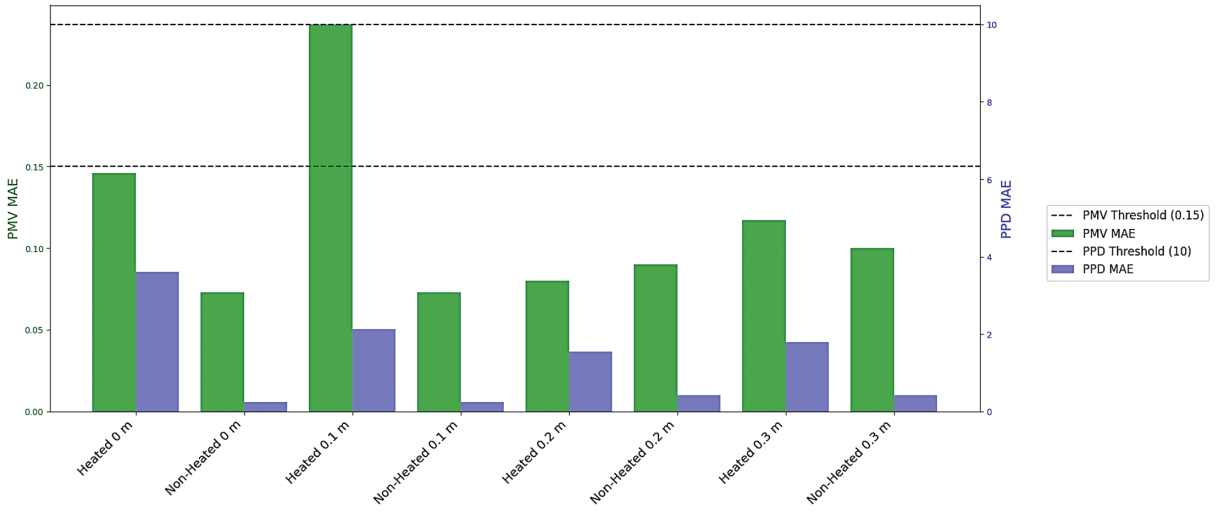

Fig. 14. PMV and PPD compliance with ISO 7730 threshold.

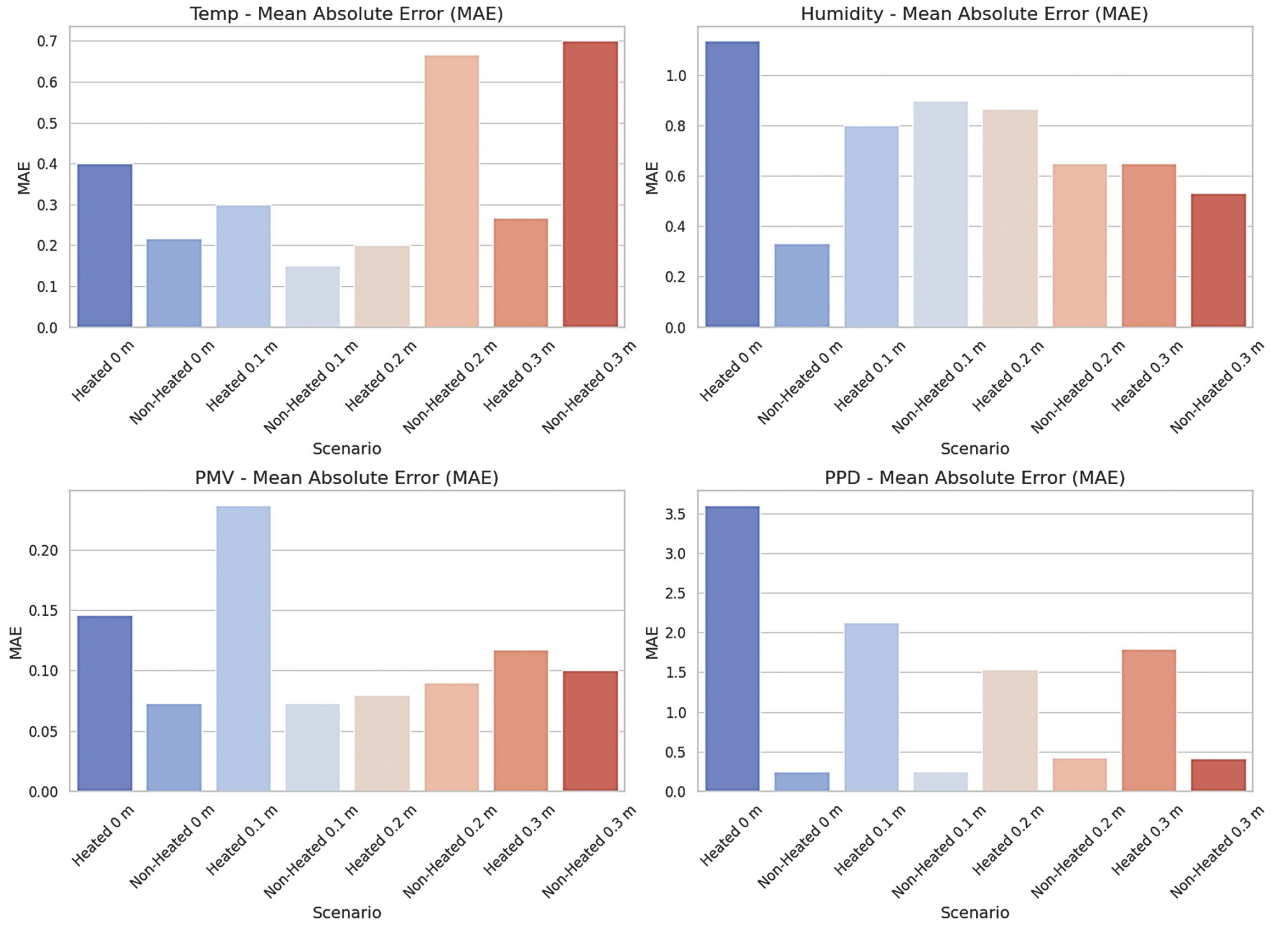

Fig. 15. Thermal comfort variables – MAE across scenarios.

heated configurations, peaking at 0.98 in the Heated 0.2 m case. Temperature R^2 followed a similar trend, reaching 0.943 in the same scenario but dropping to 0.747 in the sealed Heated 0 m condition and collapsing further in non-heated 0 m ($R^2 = -0.788$).

In contrast, humidity and PMV exhibited broader variability. Under mixed-mode regimes (0.2–0.3 m apertures), R^2 values for both clustered between 0.60 and 0.82, while low-dynamic conditions such as non-heated 0 m produced R^2 values as low as −0.788 (humidity) and 0.145 (PMV). These declines occurred despite low absolute MAEs (e.g., 0.217 °C and 0.073 PMV), indicating the inflation of normalised errors in near-steady-state environments with minimal signal variance.

In such low-variance segments, MAE/RMSE provide the more reliable indication of agreement and R^2 is treated

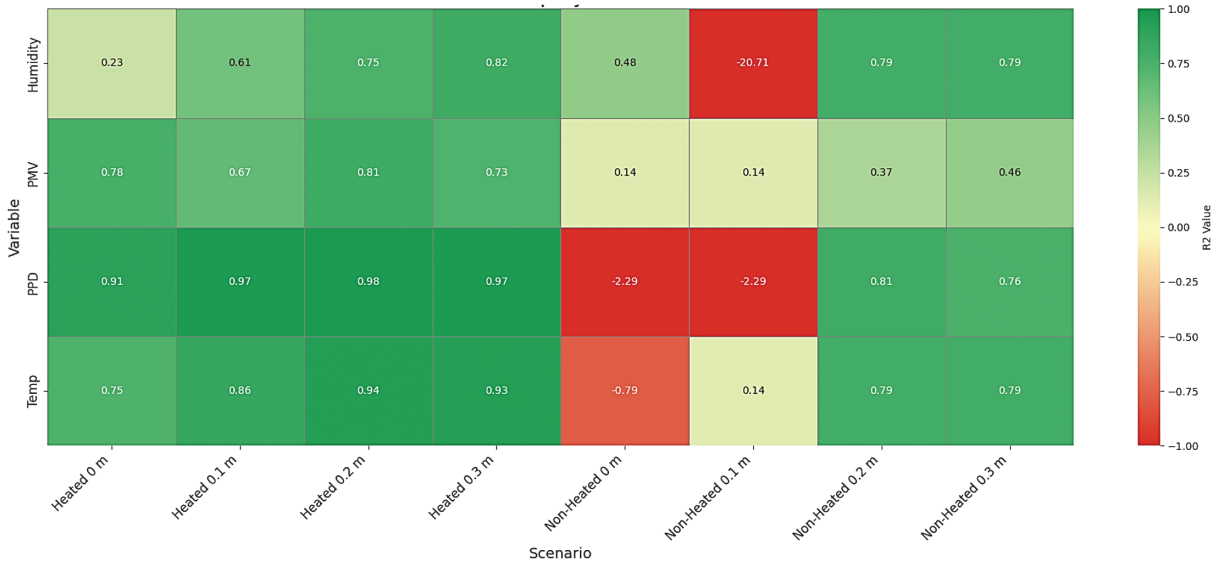

Fig. 16. R^2 correlation heatmap by scenario and variable.

as non-informative under the variance-gated reporting rule adopted in this study.

D. STATISTICAL EQUIVALENCE (WILCOXON SIGNED-RANK TEST)

Wilcoxon signed-rank tests ($\alpha = 0.05$) revealed statistically significant differences in 53% of variable–scenario pairs (17 out of 32) as shown in Fig. 17. The majority of these occurred in humidity (7 out of 8 cases), while temperature accounted for 50% of its comparisons (4 out of 8). In contrast, PMV and PPD metrics exhibited stronger equivalence to physical measurements, with only 2 PMV and 4 PPD pairs registering p-values below the significance threshold.

The most pronounced divergence was observed in the Heated 0 m scenario, where all three variables temperature, humidity, and PPD showed $p = 0.008$, consistent with the effects of delayed thermal and ventilation dynamics under sealed conditions. Conversely, non-heated scenarios such as 0.1 m and 0.3 m returned the highest p-values (e.g., PMV $p = 0.89$, humidity $p = 1$), indicating minimal residual error and reinforcing the DT system's accuracy under low-energy, steady-state conditions.

E. SYSTEM LATENCY

The DT framework exhibited a layered latency architecture, with distinct delays embedded across sensing, transmission, computation, and actuation stages each contributing to the overall responsiveness profile. At the low-level control interface, the system achieved a near-instantaneous latency of 0.2422 seconds, comprising 0.2 seconds for wireless sensor-to-DT transmission and 0.0422 seconds for encrypted actuator execution. This responsiveness exceeded the standard operational threshold of ≤ 5 seconds by over 95%, validating its suitability for real-time actuation scenarios.

However, the total latency across the complete DT cycle including CFD computation, PMV/PPD evaluation, and actuation control averaged between 6 and 7 minutes per full update. This extended cycle time reflected the computational demands of simulation-based decision-making rather than hardware limitations. Collectively, these

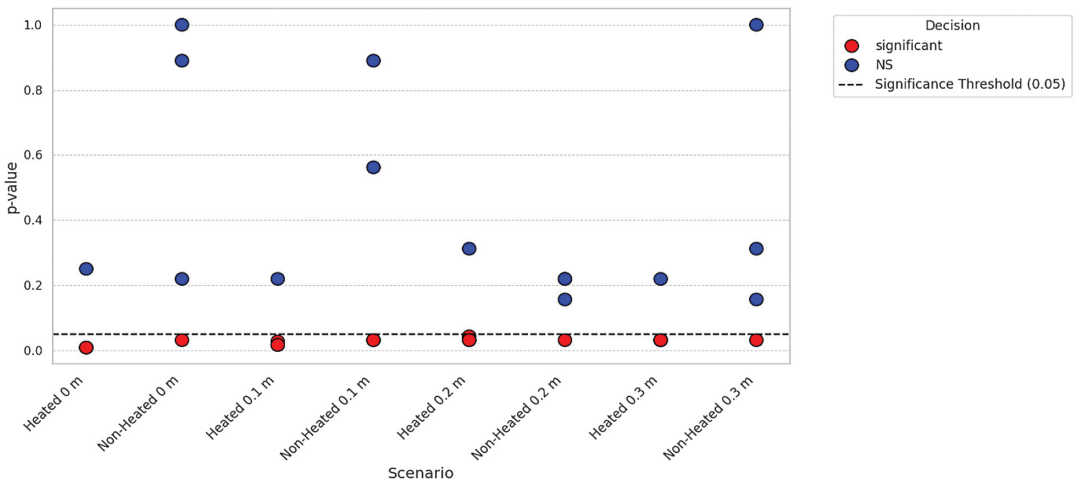

Fig. 17. Wilcoxon signed-rank test p-values across scenarios.

findings affirm the system's responsiveness at both hardware and algorithmic levels, with real-time actuation accuracy and broader predictive control capabilities.

F. LOCAL-TO-GLOBAL ACCURACY RATIO

To assess sensor-model alignment, RMSE values were normalised against sensor tolerances (Fig. 18). Across 32 variable–scenario pairs, 30 (94%) achieved compliance with their respective thresholds (Ratio $\leq$ 1). Temperature predictions met the $\pm$ 0.5 °C criterion in 14 out of 16 cases, with exceptions at non-heated 0.2 m and 0.3 m, where ratios reached 1.36 and 1.42, respectively. Humidity predictions were uniformly compliant, with all ratios $\leq$ 0.61 well below the $\pm$ 2% RH benchmark.

PMV and PPD maintained full compliance with their ISO tolerances ($\pm$ 0.3 PMV, $\pm$ 5% PPD), with the lowest error alignment observed in the non-heated 0 m and 0.1 m configurations (PPD ratios $\leq$ 0.062). The Heated 0.2 m scenario yielded the most balanced overall performance, with temperature and humidity ratios of 0.476 and 0.482, respectively. These results confirm that the DT system preserves high local-to-global accuracy across ventilation strategies, with minimal deviation from sensor-grounded truth.

G. OPERATIONAL RANGE ENVELOPE

To evaluate predictive reliability across operating points, performance is assessed using RMSE as the primary absolute-error criterion, while R^2 is treated as a conditional indicator of tracking quality during dynamic periods. Using RMSE $\leq$ 2.0 °C, the majority of variable–scenario pairs remain within acceptable absolute error limits. In contrast, several non-heated configurations exhibit low or negative R^2 despite low RMSE, which is expected when the measured series contains very small variance over the evaluation window.

To avoid over-penalizing quasi-steady conditions, a variance-gated interpretation is applied: R^2 is emphasised only when the measured variance is meaningfully above the sensor noise floor, while MAE and RMSE are prioritized in steady segments. Under this reporting rule, heated mixed-mode cases remain the strongest examples of dynamic tracking performance, while non-heated cases demonstrate strong steady-state accuracy even where correlation-based indicators are not informative. The resulting operational-range envelope across the 32 variable–scenario points is shown in Fig. 19.

H. ENERGY EFFICIENCY EVALUATION

Energy efficiency performance was assessed using the thermal conditioning energy saving equation. Results showed that only the non-heated 0 m and 0.1 m scenarios yielded positive savings of + 0.05% and + 0.04%, respectively, thereby meeting the compliance threshold (Fig. 20). In contrast, all heated configurations resulted in negative savings, with efficiency losses ranging from −6.81% to −7.97%. The highest energy penalty was observed in the Heated 0.3 m condition, consistent with enhanced buoyancy-driven infiltration under open-window heating.

I. COST EFFICIENCY (CE) EVALUATION

To assess economic viability, CE was computed for both the locally assembled sensing system (£207.90) and a commercially manufactured reference setup (£1800).

Among all evaluated conditions (0 m to 0.3 m apertures under heated and non-heated modes), only the 0 m and 0.1 m non-heated scenarios produced positive CE values. The local system recorded CE values of + 0.00024 and + 0.00019, outperforming the manufactured setup, which yielded only + 0.00003 and + 0.00002, respectively. These results highlight the superior return on investment in modular, low-cost DT systems in passive ventilation regimes.

Conversely, all heated scenarios exhibited negative CE values across both platforms, with the local system reaching −0.03834 at 0.3 m, confirming that active heating under buoyancy-driven infiltration incurs an energy cost that outweighs potential benefits. Although the manufactured system demonstrated slightly smaller negative CE values due to its higher capital investment, it never outperformed the local system under non-heated conditions.

However, this interpretation should be limited to initial deployment affordability, as full lifecycle viability would also depend on software, computation, maintenance, and calibration requirements over longer operating periods.

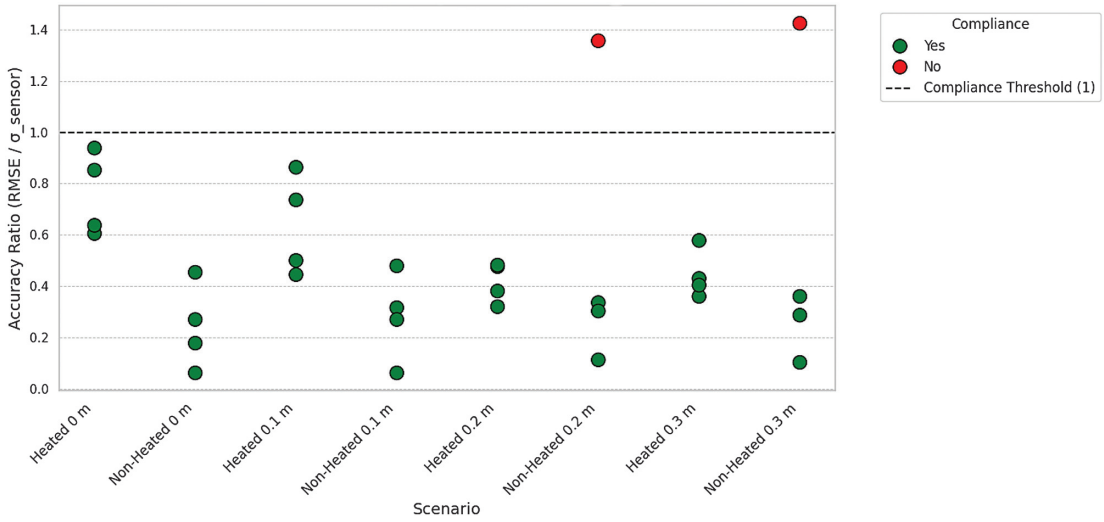

Fig. 18. Local-to-global accuracy ratio $(\mathrm{RMSE}/\sigma_{\mathrm{sensor}})$.

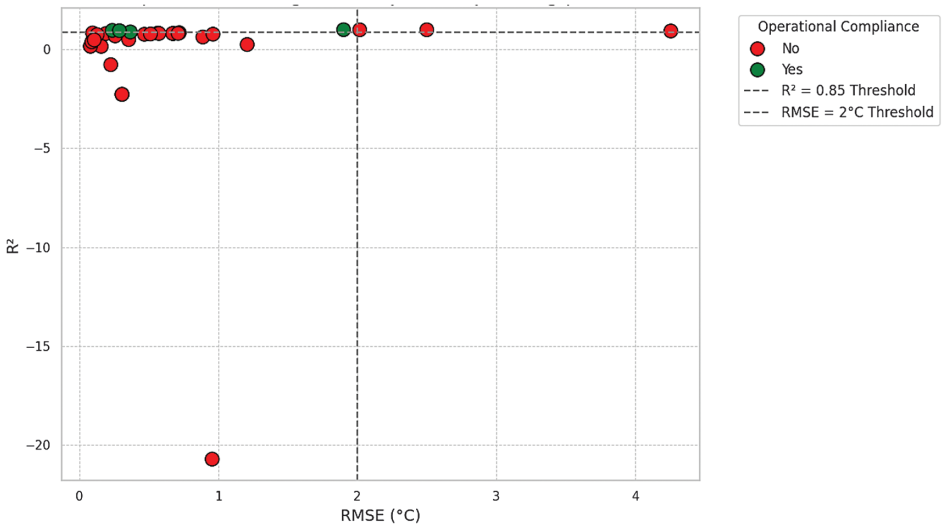

Fig. 19. Operational-range envelope (32 operating points).

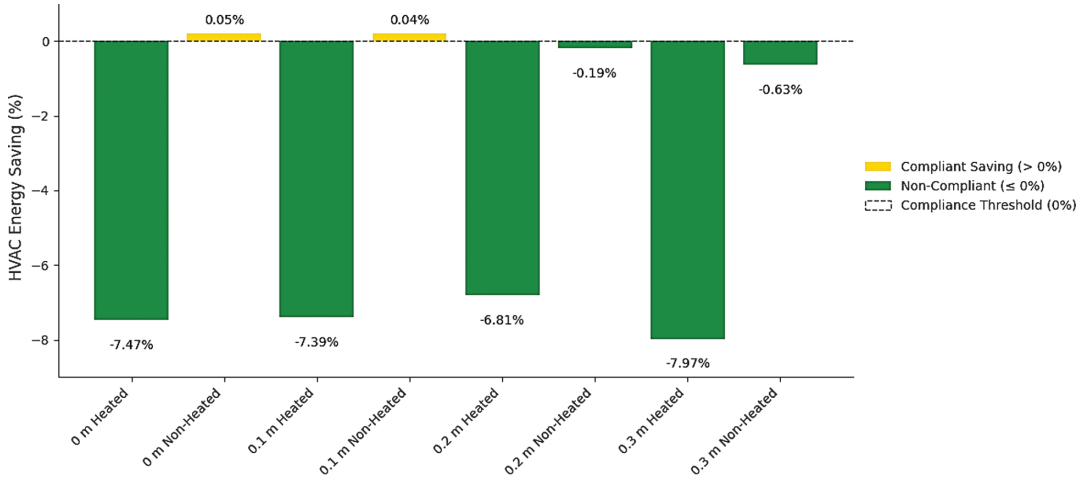

Fig. 20. Thermal conditioning energy saving percentages across window-opening configurations (0–0.3 m).

IV. DISCUSSION

A. VENTILATION STRATEGY AS A DETERMINANT OF COMFORT COMPLIANCE

DT's thermal performance was closely linked to ventilation aperture settings, especially in heated scenarios. At 0.1 m aperture under heating, PMV-MAE reached 0.237 exceeding the ISO 7730 Class A threshold of 0.15 indicating convective stratification and delayed thermal conditioning response. In contrast, wider apertures (≥ 0.2 m) consistently reduced PMV errors to ≤ 0.12 (e.g., 0.08 at Heated 0.2 m and 0.117 at Heated 0.3 m), demonstrating the effectiveness of buoyancy-driven airflow in mitigating thermal overshoot [34].

Importantly, all configurations achieved full compliance with the PPD-MAE threshold ($< 10\%$), confirming the DT's reliability in capturing occupant discomfort metrics. The non-heated 0 m condition yielded the best performance (PMV-MAE = 0.073), indicating suitability for net-zero and passive ventilation applications. However, low variance in some static conditions (e.g., $R^2 = -0.788$ for temperature at non-heated 0 m) underscores the limitations of correlation-based validation and supports the inclusion of error-based metrics in low-dynamic environments.

B. RECONCILING STATISTICAL SIGNIFICANCE WITH OCCUPANT-CENTRIC PERFORMANCE

The Wilcoxon signed-rank analysis revealed a divergence between statistical and perceptual validity. Approximately 69% of temperature and humidity comparisons exhibited statistically significant deviations ($p \leq 0.05$), yet only 25% of PMV and 50% of PPD cases were significant, with most occupant-centric metrics remaining statistically indistinguishable from reality ($p \geq 0.21$). This aligns with concerns in building simulation literature, where significance thresholds may overstate performance gaps that fall within acceptable comfort ranges [35].

In the Heated 0 m scenario, the model yielded a statistically significant temperature MAE of 0.40 °C ($p = 0.008$), which remained within ASHRAE's comfort range (± 1.0 °C), considering the sensor resolution

(± 0.5 °C). This reinforces the DTs effectiveness in prioritizing perceptual comfort through PMV/PPD rather than purely physical metrics. However, persistent offsets in sealed conditions suggest a need for adaptive recalibration mechanisms to improve alignment between numerical simulation and control behavior.

C. ADDRESSING LOW-VARIANCE VALIDATION CHALLENGES

The R^2 and operational-range results revealed critical limitations of correlation-based metrics in low-dynamic environments. Several non-heated scenarios, particularly at 0 m aperture, exhibited extremely low or negative R^2 values (e.g., $R^2 = -0.788$ for temperature and -20.711 for humidity), despite maintaining low RMSEs ($\leq$ 0.3 °C). This paradox, where predictive accuracy appears degraded under conditions of minimal thermal fluctuation, reflects the inflation of normalised errors when variance approaches zero, as demonstrated in calibrated simulation studies of low-dynamic environments [36].

To mitigate this, variance-sensitive alternatives such as Nash–Sutcliffe efficiency or reliance on absolute MAE thresholds are recommended for validation in steady-state regimes. Additionally, applying a minimum 0.2 m aperture in passive conditions would enhance dynamic response. Indeed, scenarios at this aperture consistently achieved $R^2 \geq 0.75$ across most variables (e.g., PMV $R^2 = 0.814$, PPD $R^2 = 0.81$), suggesting that modest increases in flow variability can restore correlation-based interpretability without requiring model retraining.

D. SUB-SECOND LATENCY AND SECURE EDGE CONTROL IN SMART THERMAL CONDITIONING SYSTEM

The DT framework achieved sub-second latency at the edge-control level, with an average response time of 0.2422 seconds, comprising approximately 0.2 seconds for wireless data transmission and 0.0422 seconds for actuator execution. This significantly outperformed benchmark thermal control-DT implementations, such as those reported by Mohammadi et al. (2025), which demonstrated actuation delays of approximately 1.8 seconds. This rapid responsiveness was enabled by ESP32-based edge control, a configuration validated for ultra-low-latency actuation in DT environments (Iqbal and Mirzabegi, 2025).

While this edge-level control response met stringent operational latency thresholds ($\leq$ 5 s), the full DT feedback loop including CFD computation and PMV-based control logic averaged between 6 and 7 minutes per complete cycle. Although unsuitable for fast real-time loop closure, this extended latency supports accurate predictive decision-making and long-horizon thermal strategies. The integration of secure, decentralised actuation with near-instantaneous edge response affirms the viability of the system for low-cost, scalable, and autonomous deployment in smart residential environments

E. ENERGY-CE TRADE-OFFS IN PASSIVE AND HEATED CONDITIONS

Energy performance assessment revealed that only the 0 m and 0.1 m non-heated configurations achieved positive savings (+ 0.05% and + 0.04%, respectively), thereby meeting the compliance threshold. In contrast, all heated scenarios yielded negative savings ranging from −6.81% to −7.97%, with the greatest energy penalty observed at 0.3 m under active heating. These losses are attributed to enhanced infiltration under buoyancy effect, which increased thermal system load demand despite partial ventilation [37].

Economic performance, evaluated through the CE metric, reinforced these findings. The locally assembled sensing system (£207.90) outperformed a commercially manufactured alternative (£1800) in both compliant cases, delivering CE values of + 0.00024 (0 m) and + 0.00019 (0.1 m) versus + 0.00003 and + 0.00002, respectively [38]. While the manufactured system incurred lower proportional losses in heated scenarios due to its higher baseline cost, it failed to surpass the local setup in any configuration with positive energy savings.

F. RESEARCH CONTRIBUTION

This study advances DT applications in residential environments by delivering a validated, real-time system that integrates thermal comfort compliance, predictive accuracy, latency control, and practical deployment assessment. The experimental comparison is primarily against a baseline sensor-only rule-based controller and ISO 7730 comfort criteria, which is appropriate for testing whether the DT can reproduce measured room response and maintain acceptable comfort conditions.

To place the contribution in context, the proposed framework can also be considered alongside representative alternatives commonly used in homes. Commercial smart thermostat systems typically rely on temperature set-point control using embedded logic and historical trends. They are generally easy to deploy, but they have limited spatial awareness and do not resolve room-scale airflow behavior. Model-predictive control (MPC) approaches can optimize future actions using simplified building models, but they usually require careful model identification, tuning, and reliable forecasts. In contrast, the CFD-based DT presented in this study is intended to provide spatially resolved comfort insight together with structured KPI validation, although this comes with a longer refresh time due to the computational cost of CFD.

In contrast to earlier DT studies centered on single-variable regulation or industrial contexts [39], this work evaluates eight residential ventilation scenarios using low-cost sensor arrays, CFD-enhanced forecasting, and occupant-centered thermal comfort metrics. By spanning both passive and mechanically driven modes, the study introduces a modular and scalable DT framework designed primarily for residential thermal comfort evaluation and responsive control.

G. KPI-DRIVEN FRAMEWORK

A core novelty lies in the introduction of a structured KPI framework spanning thermal accuracy, system responsiveness, statistical significance, and deployment-oriented practical evaluation. Whereas traditional DT validation methods have prioritized metrics like RMSE, this study advances a broader KPI framework that integrates PMV/PPD conformity, non-parametric significance testing (e.g., Wilcoxon), and economic efficiency indicators, an approach consistent

with emerging trends in multi-criteria DT evaluation [21]. Additionally, it responds to the shortcomings of correlation-based measures (e.g., R^2) in low-variance scenarios by proposing absolute error metrics (e.g., MAE) and sensitivity enhancements via aperture variability. This holistic validation strategy provides a replicable pathway for room-scale DT deployment in real-world residential environments, while wider household deployment will require further validation of cross-zone interactions and computational scalability.

V. CONCLUSION

This study demonstrated the practical viability and effectiveness of a structured KPI-driven DT for residential thermal comfort management and practical deployment assessment. Validation using ISO 7730 compliance (PMV and PPD), local-to-global accuracy ratios, predictive accuracy (R^2), statistical equivalence tests (Wilcoxon), and practical deployment indicators revealed strong occupant-centric performance, particularly under passive and mixed-mode conditions. Energy-related outcomes were more variable: non-heated cases showed small positive savings, whereas heated scenarios produced negative savings due to ventilation-related heat loss. These results indicate that the present system is strongest as a comfort-focused DT, while energy optimisation under heating demand would require coordinated control of both ventilation and heating.

Critical insights from KPI validation highlighted the need for adaptive control mechanisms to mitigate the limitations of correlation-based metrics (R^2) under low-dynamic conditions. The DT achieved statistically significant equivalence (53% scenario–variable significance at $\alpha = 0.05$) and demonstrated near-instantaneous responsiveness at the edge-control level (0.2422 s). While the complete DT loop incurred a longer actuation cycle (6–7 minutes), the fast edge actuation validated the system's potential for hybrid deployment modes balancing predictive control with responsive edge execution. Nevertheless, the present findings should be interpreted within the limits of a single-room testbed and fixed occupant assumptions, and broader validation across multi-zone dwellings and variable occupant conditions is still required.

A. RECOMMENDATION

In addition, selected methods emerging from cross-domain DT research, such as hybrid physics-data learning and life-cycle-aware modelling, may be adapted in future work to improve building-DT scalability and prediction robustness, provided they are reinterpreted for comfort-focused and spatially resolved residential use. However, scaling the present CFD-based framework to multi-zone or multi-story buildings is also expected to increase computation time, boundary-condition complexity, and sensor-network requirements, so future deployment will likely require staged validation and more computationally efficient update strategies. Validation strategies should continue to favor absolute performance indicators (e.g., MAE, RMSE) over variance-sensitive metrics like R^2, especially in passive or quasi-steady-state environments. Future research should also explore variance-normalised or composite KPIs to support more robust performance diagnostics across diverse operating states.

Finally, the present validation is limited to a single room (Room 2) and therefore does not fully capture multi-zone airflow coupling, stairwell exchange, or whole-house thermal interactions. Extending the framework to multiple rooms, larger buildings, or different climates will be essential for confirming practical relevance, although the low-cost, modular architecture demonstrated here provides a practical starting point for such staged deployment.

CONFLICT OF INTEREST STATEMENT

The authors declare no conflicts of interest.

REFERENCES

[1] H. Hosamo *et al.*, "Building performance optimization through sensitivity analysis, and economic insights using AI," *Energy Build.*, vol. 325, p. 114999, Dec. 2024, DOI. 10.1016/j.enbuild.2024.114999.

[2] I. Stipanovic *et al.*, "Inspection and maintenance KPIs to support decision making integrated into digital twin tool," *ce/papers,* vol. 6, no. 5, pp. 1234–1241, Sep. 2023, DOI: 10.1002/cepa.2137.

[3] S. H. Khajavi *et al.*, "Digital twin: Vision, benefits, boundaries, and creation for buildings," *IEEE Access,* vol. 7, pp. 147406–147419, 2019, DOI: 10.1109/ACCESS.2019.2946515.

[4] F. Psarommatis and G. May, "A standardized approach for measuring the performance and flexibility of digital twins," *Int. J. Prod. Res.,* vol. 61, no. 20, pp. 6923–6938, Oct. 2023, DOI: 10.1080/00207543.2022.2139005.

[5] F. Hodavand, I. J. Ramaji, and N. Sadeghi, "Digital twin for fault detection and diagnosis of building operations: A systematic review," Buildings, vol. 13, no. 6, p. 1426, May 2023, DOI: 10.3390/buildings13061426.

[6] F. Jiang *et al.*, "Transforming hospital HVAC design with BIM and digital twins: Addressing real-time use changes," *Sustainability,* vol. 17, no. 8, p. 3312, Apr. 2025, DOI: 10.3390/su17083312.

[7] F. Tao *et al.*, "Digital twin in industry: State-of-the-art," *IEEE Trans. Ind. Inform.,* vol. 15, no. 4, pp. 2405–2415, Apr. 2019, DOI: 10.1109/TII.2018.2873186.

[8] Y. Qin *et al.*, "Inverse physics–informed neural networks for digital twin–based bearing fault diagnosis under imbalanced samples," *Knowl.-Based Syst.,* vol. 292, p. 111641, May 2024, DOI: 10.1016/j.knosys.2024.111641.

[9] Y. Qin, X. Wu, and J. Luo, "Data-model combined driven digital twin of life-cycle rolling bearing," *IEEE Trans. Ind. Inform.,* vol. 18, no. 3, pp. 1530–1540, Mar. 2022, DOI: 10.1109/TII.2021.3089340.

[10] Y. Qin, H. Liu, and Y. Mao, "Faulty rolling bearing digital twin model and its application in fault diagnosis with imbalanced samples," *Adv. Eng. Inform.,* vol. 61, p. 102513, Aug. 2024, DOI: 10.1016/j.aei.2024.102513.

[11] W. Kritzinger *et al.*, "Digital twin in manufacturing: A categorical literature review and classification," *IFAC-Pap.,* vol. 51, no. 11, pp. 1016–1022, 2018, DOI: 10.1016/j.ifacol.2018.08.474.

[12] Q. Qi and F. Tao, "A smart manufacturing service system based on edge computing, fog computing, and cloud computing," *IEEE Access,* vol. 7, pp. 86769–86777, 2019, DOI: 10.1109/ACCESS.2019.2923610.

[13] C. Liu, P. Zhang, and X. Xu, "Literature review of digital twin technologies for civil infrastructure," *J. Infrastruct.*

Intell. Resil., vol. 2, no. 3, p. 100050, Sep. 2023, DOI: 10.1016/j.iintel.2023.100050.

[14] "ISO 23247-1:2021(en), Automation systems and integration — Digital twin framework for manufacturing — Part 1: Overview and general principles," [Online]. Available: https://www.iso.org/obp/ui/en/#iso:std:iso:23247:-1:ed-1:v1:en, Accessed on: Jan. 08, 2026.

[15] F. Stadtmann *et al.*, "Physics-guided federated learning as an enabler for digital twins," *Expert Syst. Appl.,* vol. 258, p. 125169, Dec. 2024, DOI: 10.1016/j.eswa.2024.125169.

[16] A. Kusiak, "Smart manufacturing," *Int. J. Prod. Res.,* vol. 56, no. 1–2, pp. 508–517, Jan. 2018, DOI: 10.1080/00207543.2017.1351644.

[17] Y. Wang *et al.*, "An intelligent and privacy-preserving digital twin model for aging-in-place," *arXiv*: Apr. 04, 2025, arXiv:2504.03798. DOI: 10.48550/arXiv.2504.03798.

[18] S. Mazzetto, "Dynamic integration of shading and ventilation: Novel quantitative insights into building performance optimization," *Buildings.,* vol. 15, no. 7, p. 1123, Mar. 2025, DOI: 10.3390/buildings15071123.

[19] A. Buonomano *et al.*, "Optimizing building performance: A novel digital twin framework for enhanced thermal comfort," in *2024 3rd International Conference on Energy Transition in the Mediterranean Area (SyNERGY MED)*, Limassol, Cyprus: IEEE, Oct. 2024, pp. 1–5. DOI: 10.1109/SyNERGYMED62435.2024.10799267.

[20] H. H. Hosamo *et al.*, "Improving building occupant comfort through a digital twin approach: A Bayesian network model and predictive maintenance method," *Energy Build.,* vol. 288, 2023, DOI: 10.1016/j.enbuild.2023.112992.

[21] F. Iqbal and S. Mirzabeigi, "Digital twin-enabled building information Modeling–Internet of Things (BIM-IoT) framework for optimizing indoor thermal comfort using Machine Learning," *Buildings.*, vol. 15, no. 10, p. 1584, May 2025, DOI: 10.3390/buildings15101584.

[22] G. Piras, S. Agostinelli, and F. Muzi, "Smart buildings and digital twin to monitoring the efficiency and wellness of working environments: A case study on IoT integration and data-driven management," *Appl. Sci.*, vol. 15, no. 9, p. 4939, Apr. 2025, DOI: 10.3390/app15094939.

[23] A. Zaballos *et al.*, "A smart campus' digital twin for sustainable comfort monitoring," *Sustainability*, vol. 12, no. 21, p. 9196, Nov. 2020, DOI: 10.3390/su12219196.

[24] G. Desogus *et al.*, "From building information model to digital twin: A framework for building thermal comfort monitoring, visualizing, and assessment," *Buildings.*, vol. 13, no. 8, p. 1971, Aug. 2023, DOI: 10.3390/buildings13081971.

[25] M. Elnour *et al.*, "Empowering smart cities with digital twins of buildings: Applications and implementation considerations of data-driven energy modelling in building management," *Build. Serv. Eng. Res. Technol.*, vol. 45, no. 4, pp. 475–498, Jul. 2024, DOI: 10.1177/01436244241239290.

[26] M. Stogia *et al.*, "A scalable and user-friendly framework integrating IoT and digital twins for home energy management systems," *Appl. Sci.*, vol. 14, no. 24, p. 11834, Dec. 2024, DOI: 10.3390/app142411834.

[27] I. Petri *et al.*, "Digital twins for performance management in the built environment," *J. Ind. Inf. Integr.*, vol. 33, p. 100445, Jun. 2023, DOI: 10.1016/j.jii.2023.100445.

[28] K. Wang *et al.*, "Digital twin-assisted service function chaining in multi-domain computing power networks with multi-agent reinforcement learning," *Future Gener. Comput. Syst.*, vol. 158, pp. 294–307, 2024, DOI: 10.1016/j.future.2024.04.025.

[29] M. Aderibigbe, A. M. Aliyu, and R. Mishra, "Aerosol Dispersion in Ventilated Rooms: Effect of Built Space Configuration and Facemasks on Indoor Transmission," in *Proceedings of the UNIfied Conference of DAMAS, IncoME and TEPEN Conferences (UNIfied 2023)*, Springer, Cham, 2024, pp. 1149–1164. DOI: 10.1007/978-3-031-49421-5_94.

[30] A. M. Aliyu *et al.*, "Dispersion of virus-laden droplets in ventilated rooms: Effect of homemade facemasks," *J. Build. Eng.*, vol. 44, p. 102933, Dec. 2021, DOI: 10.1016/j.jobe.2021.102933.

[31] M. I. Alhassan *et al.*, "Air Quality Management in Railway Coaches," in *2021 International Conference on Maintenance and Intelligent Asset Management (ICMIAM)*, Ballarat, Australia: IEEE, Dec. 2021, pp. 1–5. DOI: 10.1109/ICMIAM54662.2021.9715208.

[32] A. M. Aliyu *et al.*, "Dispersion of virus-laden droplets in ventilated rooms: Effect of homemade facemasks," *J. Build. Eng.*, vol. 44, p. 102933, Dec. 2021, DOI: 10.1016/j.jobe.2021.102933.

[33] S. Yoo and K. Ito, "Validation, verification, and quality control of computational fluid dynamics analysis for indoor environments using a computer-simulated person with respiratory tract," *Jpn. Archit. Rev.*, vol. 5, no. 4, pp. 714–727, Oct. 2022, DOI: 10.1002/2475-8876.12301.

[34] Z. ElArwady *et al.*, "Modeling indoor thermal comfort in buildings using digital twin and machine learning," *Dev. Built Environ.*, vol. 19, p. 100480, Oct. 2024, DOI: 10.1016/j.dibe.2024.100480.

[35] T. Cheung *et al.*, "Analysis of the accuracy on PMV – PPD model using the ASHRAE global thermal comfort database II," *Build. Environ.*, vol. 153, pp. 205–217, Apr. 2019, DOI: 10.1016/j.buildenv.2019.01.055.

[36] G. B. A. Coelho, H. E. Silva, and F. M. A. Henriques, "Calibrated hygrothermal simulation models for historical buildings," *Build. Environ.*, vol. 142, pp. 439–450, Sep. 2018, DOI: 10.1016/j.buildenv.2018.06.034.

[37] H. H. Hosamo *et al.*, "Improving building occupant comfort through a digital twin approach: A Bayesian network model and predictive maintenance method," *Energy Build.*, vol. 288, p. 112992, Jun. 2023, DOI: 10.1016/j.enbuild.2023.112992.

[38] A. Salzano *et al.*, "HVAC system performance in educational facilities: A case study on the integration of digital twin technology and IoT sensors for predictive maintenance," *J. Archit. Eng.*, vol. 31, no. 1, p. 04025004, Mar. 2025, DOI: 10.1061/JAEIED.AEENG-1855.

[39] L. Zhao *et al.*, "Overview of digital twin-driven rotating machinery fault diagnosis: Status and trends," *Meas. Sci. Technol.*, vol. 36, no. 5, p. 052001, Apr. 2025, DOI: 10.1088/1361-6501/adc8c3.